

Bayesian graphical modelling for heterogeneous causal effects

Federico Castelletti ^{*1} and Guido Consonni ^{†2}

^{1,2}Department of Statistical Sciences, Università Cattolica del Sacro Cuore, Milan

Abstract

Our motivation stems from current medical research aiming at personalized treatment using a molecular-based approach. The goal is to develop a more precise and targeted decision making process, relative to traditional treatments based primarily on clinical diagnoses. A challenge we address is evaluating treatment effects for individuals affected by Glioblastoma (GBM), a brain cancer where targeted therapy is essential to improve patients' prospects. Specifically, we consider the pathway associated to cytokine $TGF\beta$, whose abnormal signalling activity has been found to be linked to the progression of GBM and other tumors. We analyze treatment effects within a causal framework represented by a Directed Acyclic Graph (DAG) model, whose vertices are the variables belonging to the $TGF\beta$ pathway. A major obstacle in implementing the above program is represented by individual heterogeneity, implying that patients will respond differently to the same therapy. We address this issue through an infinite mixture of Gaussian DAG-models where both the graphical structure as well as the allied model parameters are regarded as uncertain. Our procedure determines a clustering structure of the units reflecting the underlying heterogeneity, and produces subject-specific causal effects through Bayesian model averaging across a variety of model features. When applied to the GBM dataset, it reveals that regulation of $TGF\beta$ proteins produces heterogeneous effects, represented by clusters of patients potentially benefiting from selective interventions.

Keywords: Bayesian model averaging; Directed acyclic graph; Dirichlet process mixture; Personalized treatment; Tumor heterogeneity.

1 Introduction

1.1 Background and Motivation

Heterogeneity of individual responses to treatment is a pervasive aspect in a variety of clinical domains. An example is cancer which is not a single disease as it involves subtypes character-

^{*}federico.castelletti@unicatt.it

[†]guido.consonni@unicatt.it

ized by distinct sets of molecules; this implies that patients will react differently to the same treatment. Currently the best treatment is identified based on clinical diagnoses as opposed to a molecular-based approach which would allow a more precise and targeted approach to decision making, leading to better treatments and eventually more favorable prognoses. At present there exists a variety of methods to identify cancer subtypes [40, 35]; however they cannot establish whether subtypes show heterogeneous responses toward a treatment. Identifying subtypes with heterogeneous treatment effects is a causal problem that need be addressed for a more informed decision strategy [43].

In this paper we analyze a dataset concerning patients affected by Glioblastoma (GBM). There exists two broad clinical classes of GBM: primary (which represents 90% of all cases), and secondary. In particular, primary GBM is a brain cancer which responds very poorly to treatment (average survival time is around 14-15 months from diagnosis). The development of new targeted treatments is therefore required to improve patients' prospects. Cytokine $TGF\beta$ is known to play a variety of functions ranging from tissue repair to immune response. Its abnormal signaling activity has been associated to the development and progression of many tumor types including GBM. The targeting of $TGF\beta$ signalling is thus considered a potentially promising therapy; see Birch et al. [5] for an excellent review. Thanks to advanced sequencing and transcriptional profiling technology it has become apparent that GBM cells exhibit significant inter- and intra-tumor heterogeneity [28]. This can be a source of treatment failure, together with other factors (e.g. the presence of Gliostem cells populations). Oncogenic $TBF\beta$ is known to impact the development of GBM through a growth factor addition. Hence identifying $TBF\beta$ inhibitors is of great value to develop targeted therapies.

We apply our methodology to the $TBF\beta$ -pathway comprising twenty variables observed over seventy patients. We investigate the existence of clustering characterized by differential graph structures as well as model parameter configurations, and evaluate a battery of causal effects on selected $TBF\beta$ responses. We then pair clusters with heterogeneity of causal effects, and identify broad patterns of potential use for targeted therapy.

1.2 Overview of our Model

In this subsection we provide the broad picture underlying our model, while leaving technical specifications to later sections. In our setup we have a collection of variables $\{X_1, \dots, X_q\}$, exemplified by the gene expressions in the $TGF\beta$ pathway. When we are interested in isolating one of the variables as a response we label it as Y . We consider a sample of size n from the q -dimensional population. To account for potential heterogeneity of the subjects we assume that the statistical model is a mixture of Directed Acyclic Graph (DAG) models. This means that, if we knew the mixture component of the unit, its distributional family would factorize according to the corresponding DAG, equivalently it would be *Markov* with respect to that

DAG. Graphical models [20] are very effective for encoding conditional independencies. In our setting however we view a DAG as a causal model [29]; in particular this means that the joint *interventional* distribution of the variables, following a hypothetical intervention on a variable in the system, would still be Markov relative to the DAG, save for the component subjected to intervention, which will be specified separately. This stability assumption is crucial to define the notion of total causal effect on Y following an intervention on X_j [23].

From a modeling perspective, we start by assuming that the joint observational distribution belongs to a Dirichlet Process (DP) mixture of Gaussian DAG models; see Müller & Mitra [25] for an overview of DP mixtures. The mixing measure is over the space of priors on $(\boldsymbol{\mu}, \boldsymbol{\Omega}, \mathcal{D})$ where \mathcal{D} is a DAG and $(\boldsymbol{\mu}, \boldsymbol{\Omega})$ the parameters of a q -variate Normal distribution having precision $\boldsymbol{\Omega} \in \mathcal{P}_{\mathcal{D}}$, where $\mathcal{P}_{\mathcal{D}}$ is the space of symmetric and positive-definite matrices constrained by being Markov relative to \mathcal{D} . We take the baseline measure of the DP as $p(\boldsymbol{\mu}, \boldsymbol{\Omega} | \mathcal{D})p(\mathcal{D})$, and specify $p(\boldsymbol{\mu}, \boldsymbol{\Omega} | \mathcal{D})$ as a Normal-DAG-Wishart prior after a suitable reparameterization involving a Cholesky-type decomposition of $\boldsymbol{\Omega}$ [6]. We employ a constructive procedure which produces a prior under *any* DAG model based on the elicitation of a *single* standard Normal-Wishart prior on $(\boldsymbol{\mu}, \boldsymbol{\Omega})$, with $\boldsymbol{\Omega}$ unconstrained. In this way, not only is the elicitation procedure drastically simplified, but the marginal likelihood of DAGs belonging to the same Markov class can be shown to be constant (score equivalence), besides being available in closed form. Computations for our model are performed through an MCMC strategy based on a slice sampler [39] and the Partial Analytic Structure (PAS) algorithm of Godsill [16].

Our contribution can be summarized as follows. We provide a Bayesian modeling framework to evaluate heterogeneous causal effects based on Directed Acyclic Graphs. Specifically, our model: i) accounts for individual heterogeneity through an infinite mixture model; ii) allows for structure (DAG) and parameter uncertainty; iii) determines a clustering structure of the units; iv) produces subject-specific causal effects incorporating uncertainty on various aspects of the model through Bayesian model averaging.

When applied to the Glioblastoma data it highlights that regulation of $\text{TGF}\beta$ proteins induced by gene therapy produces heterogeneous effects, and identifies cluster of patients potentially benefiting from selective interventions.

1.3 Related work

The literature on the analysis of heterogeneous causal effects has been growing lately, especially in the machine learning community where tree-based methods, in particular random forests, have found natural applications. Works in this area have been carried out mostly within the potential outcome framework [33]; see for instance Athey & Imbens [1], Wager & Athey [38], Lee et al. [21] and Hahn et al. [17] for a Bayesian viewpoint.

A more decision theoretic approach is presented in Shpitser & Sherman [36] who discuss

identification of personalized effects in causal pathways. The central idea is to overcome traditional causal inference, and explore settings where the goal is to map a unit’s characteristics to a treatment tailored to maximize the expected outcome for that unit. This line of approach is also connected to literature spanning from dynamic treatment regime to mediation analysis.

Moving to a Bayesian perspective, inference on causal effects within the causal graph framework has been traditionally carried out assuming a homogeneous population, that is the observations are (conditionally) independent and identically distributed from a zero-mean Gaussian DAG-model; see for instance Castelletti & Consonni [8] and Castelletti & Consonni [7].

So far heterogeneity has been mostly linked to differential Bayesian structural learning as in multiple graphical modeling, where each model is associated to a specific group which is known in advance; see Peterson et al. [31] and Castelletti et al. [9] for directed graphs. Also, Ni et al. [27] provide an extensions to multi-dimensional graphs. A previous important attempt to deal explicitly with heterogeneity using a DP mixture of Gaussian graphical models is Rodríguez et al. [32]. There are however notable differences with respect to our work. First of all they only consider structural and parameter learning for undirected graphs; secondly there is no discussion of causal inference. Bayesian nonparametric techniques have been used in graphical modeling also for robustness purposes: see Finegold & Drton [12, 13], and Cremaschi et al. [10] for an extension to more general measures.

We close this subsection by pointing to a more foundational line of research that connects invariance, causality and robustness [3] where an important role is played by heterogeneity; the latter however relates to different “environments”, seen and unseen, and thus has a broader scope than the notion of heterogeneity employed in this paper.

1.4 Structure of the paper

The organization of the rest of this paper is as follows. In Section 2 we provide some background results on causal effect estimation based on DAGs. We then introduce in Section 3 our DP mixture of Gaussian DAG models with particular emphasis on the specification of the baseline prior distribution for model parameters. Posterior inference is discussed in Section 4. In Section 5 we conduct extensive simulation experiments to evaluate the proposed method in terms of structural learning, clustering and causal effect estimation. Section 6 is entirely devoted to the analysis of the Glioblastoma data, highlighting the heterogeneity of causal effects as well as the clustering structure. Finally, Section 7 offers a few points for discussion. Some theoretical results on parameter prior distributions and computational details are reported in the Supplementary material. The latter also contains additional results to enrich our analysis of the Glioblastoma data.

2 Background

2.1 Directed acyclic graphs and causal effects

Let X_1, \dots, X_q be a collection of real-valued continuous random variables with joint p.d.f. $f(x_1, \dots, x_q)$. Let also $\mathcal{D} = (V, E)$ be a Directed Acyclic Graph (DAG), where $V = \{1, \dots, q\}$ is a set of nodes associated to variables X_1, \dots, X_q and $E \subseteq V \times V$ is a set of edges. If $(u, v) \in E$, then $(v, u) \notin E$ and we say that u is a *parent* of node v ; by converse we say that v is a *child* of u . The set of all parents of v in \mathcal{D} is then denoted by $\text{pa}_{\mathcal{D}}(v)$. Under DAG \mathcal{D} the joint density factorizes as

$$f(x_1, \dots, x_q | \mathcal{D}) = \prod_{j=1}^q f(x_j | \mathbf{x}_{\text{pa}_{\mathcal{D}}(j)}), \quad (1)$$

Factorization (1) is often called the Markov property and determines conditional independence relations among (set of) nodes which can be read-off from the DAG using graphical criteria. We also assume *faithfulness* of $f(\cdot)$ to \mathcal{D} which prescribes that the conditional independencies implied by (1) are exactly those graphically encoded by \mathcal{D} . We remark that faithfulness holds, up to sets of Lebesgue measure zero, under many common families of distributions such as the Gaussian model (Section 2.2).

Consider now a (deterministic) *intervention* on variable X_s which consists in setting X_s to the value \tilde{x} and is denoted as $\text{do}(X_s = \tilde{x})$. The *post-intervention* density is [29]

$$f(x_1, \dots, x_q | \text{do}(X_s = \tilde{x})) = \begin{cases} \prod_{j=1, j \neq s}^q f(x_j | \mathbf{x}_{\text{pa}_{\mathcal{D}}(j)})|_{x_s=\tilde{x}} & \text{if } x_s = \tilde{x}, \\ 0 & \text{otherwise,} \end{cases} \quad (2)$$

where, importantly, each term $f(x_j | \mathbf{x}_{\text{pa}_{\mathcal{D}}(j)})$ in (2) is the corresponding (pre-intervention) conditional density of Equation (1); this implies that the data generating mechanism is *stable* under intervention, because the latter only affects the local component distribution $f(x_s | \mathbf{x}_{\text{pa}_{\mathcal{D}}(s)})$ which is reduced to a point mass on \tilde{x} .

In particular, we are interested in evaluating the causal effect of an intervention $\text{do}(X_s = \tilde{x})$ on a response variable Y ; by convention we set $X_1 = Y$. The post-intervention distribution of Y is then obtained by integrating (2) w.r.t. x_2, \dots, x_q which simplifies to

$$f(y | \text{do}(X_s = \tilde{x})) = \int f(y | \tilde{x}, \mathbf{x}_{\text{pa}_{\mathcal{D}}(s)}) f(\mathbf{x}_{\text{pa}_{\mathcal{D}}(s)}) d\mathbf{x}_{\text{pa}_{\mathcal{D}}(s)}; \quad (3)$$

if $Y \notin \text{pa}_{\mathcal{D}}(s)$; on the other hand if $Y \in \text{pa}_{\mathcal{D}}(s)$ then $f(y | \text{do}(X_s = \tilde{x})) = f(y)$; see Pearl [29, Theorem 3.2.2]. Equation (3) uses the most common *adjustment* set, namely the set of parents of X_s ; other valid adjustment sets are however possible; see Witte et al. [41]. Also, it is common to summarize the causal effect on Y of an intervention on X_s through the derivative of the expected value of (3)

$$\gamma_s := \frac{\partial}{\partial x} \mathbb{E}(Y | \text{do}(X_s = \tilde{x}))|_{x=\tilde{x}}. \quad (4)$$

Clearly if $f(\cdot)$ belongs to some parametric family indexed by $\boldsymbol{\theta} \in \Theta_{\mathcal{D}}$ (a parameter specific to the underlying DAG), the causal effect γ_s will be a function of $\boldsymbol{\theta}$; accordingly, inference on $\boldsymbol{\theta}$ will drive inference on γ_s .

2.2 Gaussian DAG models

In the following we focus on *Gaussian* DAG models and assume

$$X_1, \dots, X_q \mid \boldsymbol{\mu}, \boldsymbol{\Omega} \sim \mathcal{N}_q(\boldsymbol{\mu}, \boldsymbol{\Omega}^{-1}), \quad (5)$$

where $\boldsymbol{\mu} = (\mu_1, \dots, \mu_q)^\top \in \mathbb{R}^q$ and $\boldsymbol{\Omega} \in \mathcal{P}_{\mathcal{D}}$, the set of all symmetric positive definite (s.p.d.) precision matrices Markov w.r.t. \mathcal{D} .

Equation (5) can be alternatively written as a Structural Equation Model (SEM). Given $\boldsymbol{\Sigma} = \boldsymbol{\Omega}^{-1}$, consider the reparameterization

$$\mathbf{L}_{\prec j]} = \boldsymbol{\Sigma}_{\prec j \succ}^{-1} \boldsymbol{\Sigma}_{\prec j]}, \quad \mathbf{D}_{jj} = \boldsymbol{\Sigma}_{jj \mid \prec j \succ}, \quad \eta_j = \mu_j + \mathbf{L}_{\prec j]}^\top \boldsymbol{\mu}_{\prec j \succ}, \quad (6)$$

for $j = 1, \dots, q$, where $\boldsymbol{\Sigma}_{jj \mid \prec j \succ} = \boldsymbol{\Sigma}_{jj} - \boldsymbol{\Sigma}_{\prec j \succ} \boldsymbol{\Sigma}_{\prec j \succ}^{-1} \boldsymbol{\Sigma}_{\prec j]}$, $\prec j \succ = \text{pa}_{\mathcal{D}}(j) \times j$, $\prec j \succ = j \times \text{pa}_{\mathcal{D}}(j)$, $\prec j \succ = \text{pa}_{\mathcal{D}}(j) \times \text{pa}_{\mathcal{D}}(j)$. Parameters $\mathbf{L}_{\prec j \succ}$'s correspond to the non-zero elements of a (q, q) matrix \mathbf{L} with all diagonal entries equal to one. Moreover, if we let \mathbf{D} be a (q, q) diagonal matrix with (j, j) -element \mathbf{D}_{jj} and $\boldsymbol{\eta} = (\eta_1, \dots, \eta_q)^\top$, the SEM representation of (5) is given by

$$\boldsymbol{\eta} + \mathbf{L}^\top (X_1, \dots, X_q)^\top = \boldsymbol{\varepsilon},$$

where $\boldsymbol{\varepsilon} \sim \mathcal{N}_q(\mathbf{0}, \mathbf{D})$. Equivalently, we can write

$$f(x_1, \dots, x_q \mid \boldsymbol{\mu}, \boldsymbol{\Omega}, \mathcal{D}) = \prod_{j=1}^q d\mathcal{N}(x_j \mid \eta_j - \mathbf{L}_{\prec j \succ}^\top \mathbf{x}_{\text{pa}_{\mathcal{D}}(j)}, \mathbf{D}_{jj}), \quad (7)$$

where $d\mathcal{N}(x \mid \mu, \sigma^2)$ denotes the Normal density of $\mathcal{N}(\mu, \sigma^2)$. Equation (7) represents the density of a Gaussian DAG model after the reparameterization $(\boldsymbol{\mu}, \boldsymbol{\Omega}) \mapsto (\boldsymbol{\eta}, \mathbf{L}, \mathbf{D})$; compare also Equation (1). Finally we note that $\boldsymbol{\Omega} = \mathbf{L} \mathbf{D}^{-1} \mathbf{L}^\top$.

Consider now the causal effect of an intervention $\text{do}(X_s = \tilde{x})$ on $Y = X_1$ as defined in Equation (4). Under the Gaussian model (5), the post-intervention distribution of Y can be written as

$$f(y \mid \text{do}(X_s = \tilde{x}), \boldsymbol{\mu}, \boldsymbol{\Omega}, \mathcal{D}) = \int f(y \mid \tilde{x}, \mathbf{x}_{\text{pa}_{\mathcal{D}}(s)}, \boldsymbol{\mu}, \boldsymbol{\Omega}) f(\mathbf{x}_{\text{pa}_{\mathcal{D}}(s)} \mid \boldsymbol{\mu}, \boldsymbol{\Omega}) d\mathbf{x}_{\text{pa}_{\mathcal{D}}(s)}, \quad (8)$$

where each density under the integral sign is a suitable Normal. Taking the expectation of the post-intervention distribution on the left-hand-side of (8), and interchanging the order of integration in the right-hand-side, one obtains

$$\mathbb{E}(Y \mid \text{do}(X_s = \tilde{x}), \boldsymbol{\mu}, \boldsymbol{\Omega}, \mathcal{D}) = \gamma_0 + \gamma_s \tilde{x} + \boldsymbol{\gamma}_{\text{pa}_{\mathcal{D}}(s)}^\top \boldsymbol{\mu}_{\text{pa}_{\mathcal{D}}(s)} \quad (9)$$

so that, using (4), the causal effect of $\text{do}(X_s = \tilde{x}_s)$ on Y is γ_s , the coefficient associated to X_s in the conditional expectation of Y given $\mathbf{x}_{\text{fa}_{\mathcal{D}}(s)}$ with $\text{fa}_{\mathcal{D}}(s) = s \cup \text{pa}_{\mathcal{D}}(s)$. Therefore, the causal effect γ_s can be retrieved from the covariance matrix $\Sigma = \Omega^{-1}$ as

$$\gamma_s = \left[[\Sigma_{Y, \text{fa}_{\mathcal{D}}(s)}] (\Sigma_{\text{fa}_{\mathcal{D}}(s), \text{fa}_{\mathcal{D}}(s)})^{-1} \right]_1 \quad (10)$$

where subscript 1 refers to the first element of the vector.

3 Dirichlet process mixture of Gaussian DAG models

We consider a Dirichlet Process (DP) mixture of Gaussian DAG models so that

$$\begin{aligned} X_1, \dots, X_q \mid H &\sim \int f(x_1, \dots, x_q \mid \mu, \Omega, \mathcal{D}) H(d\mu, d\Omega, d\mathcal{D}) \\ H &\sim \text{DP}(\alpha_0, M), \end{aligned} \quad (11)$$

where $f(x_1, \dots, x_q \mid \mu, \Omega, \mathcal{D})$ denotes the density of a Gaussian DAG model defined in (7), and H follows a DP with parameters α_0 (precision) and M (baseline), written $H(\cdot) \sim \text{DP}(\alpha_0, M)$. With regard to the baseline measure we set

$$M(d\mu, d\Omega, d\mathcal{D}) = p(\mu, \Omega \mid \mathcal{D}) p(\mathcal{D}) d\mu d\Omega d\mathcal{D}, \quad (12)$$

where priors $p(\mu, \Omega \mid \mathcal{D})$ and $p(\mathcal{D})$ will be shortly defined in Section 3.1.

Let now $\mathbf{x}_i = (x_{i,1}, \dots, x_{i,q})^\top$, $i = 1, \dots, n$, be n independent draws from (11). Recall that in a DP mixture each sample \mathbf{x}_i , $i = 1, \dots, n$, has potentially a distinct parameter $\theta_i = (\mu_i, \Omega_i, \mathcal{D}_i)$. Let $K \leq n$ be the number of unique values among $\theta_1, \dots, \theta_n$ and ξ_1, \dots, ξ_n a sequence of indicator variables, with $\xi_i \in \{1, \dots, K\}$, such that $\theta_i = \theta_{\xi_i}^*$. Denote now with \mathbf{X} the (n, q) data matrix obtained by row-binding the individual observations \mathbf{x}_i^\top 's. It is instructive to write the DP mixture models in terms of the random partition induced by the $\{\xi_i\}$'s,

$$f(\mathbf{X} \mid \xi_1, \dots, \xi_n, K) = \prod_{k=1}^K \left\{ \int \left[\prod_{i: \xi_i=k} f(\mathbf{x}_i \mid \mu_k^*, \Omega_k^*, \mathcal{D}_k^*) \right] M(d\mu_k^*, d\Omega_k^*, d\mathcal{D}_k^*) \right\}. \quad (13)$$

Representation (13) is easily interpretable. The model groups observations into homogeneous classes, with samples within each class generated from a standard Gaussian DAG model. In practice, for a given partition, \mathbf{X} is split into K sub-matrices $\mathbf{X}^{(k)}$, $k = 1, \dots, K$, each $\mathbf{X}^{(k)}$ collecting all observations \mathbf{x}_i such that $\xi_i = k$.

3.1 Prior on DAG parameters

We now detail our choice of prior distributions $p(\mu, \Omega \mid \mathcal{D})$ and $p(\mathcal{D})$.

For a given DAG \mathcal{D} , let $(\boldsymbol{\mu}, \boldsymbol{\Omega})$ be the corresponding parameters, where $\boldsymbol{\mu} \in \mathbb{R}^q$, $\boldsymbol{\Omega} \in \mathcal{P}_{\mathcal{D}}$. We first consider the reparameterization $(\boldsymbol{\mu}, \boldsymbol{\Omega}) \mapsto (\boldsymbol{\eta}, \mathbf{L}, \mathbf{D})$ introduced in Section 2.2. Our elicitation procedure relies on the method of Geiger & Heckerman [15]. A main feature of this approach is that we only need to specify a prior for the parameters of a *complete* DAG model, $\mathcal{N}_q(\boldsymbol{\mu}, \boldsymbol{\Omega}^{-1})$, with $\boldsymbol{\Omega} \in \mathcal{P}$ *unconstrained*; the prior for any other (incomplete) DAG is then derived automatically, as we detail in the Supplementary material. Additionally, and importantly, this procedure guarantees *compatibility* of priors in the sense that Markov equivalent DAGs are scored with the same marginal likelihood. Specifically, we show that a Normal-Wishart prior, $(\boldsymbol{\mu}, \boldsymbol{\Omega}) \sim \mathcal{N}\mathcal{W}(a_{\mu}, \mathbf{m}, a_{\Omega}, \mathbf{U})$, leads to the compatible prior

$$\begin{aligned} p(\boldsymbol{\eta}, \mathbf{D}, \mathbf{L} | \mathcal{D}) &= \prod_{j=1}^q p(\eta_j, \mathbf{L}_{\prec j}], \mathbf{D}_{jj}) \\ &= \prod_{j=1}^q p(\eta_j | \mathbf{L}_{\prec j}], \mathbf{D}_{jj}) p(\mathbf{L}_{\prec j}] | \mathbf{D}_{jj}) p(\mathbf{D}_{jj}) \end{aligned} \quad (14)$$

where

$$\begin{aligned} \mathbf{D}_{jj} &\sim \text{I-Ga} \left(\frac{1}{2} a_j^{\mathcal{D}}, \frac{1}{2} \mathbf{U}_{jj | \prec j \succ} \right), \\ \mathbf{L}_{\prec j}] | \mathbf{D}_{jj} &\sim \mathcal{N}_{|\text{pa}_{\mathcal{D}}(j)|} \left(-\mathbf{U}_{\prec j \succ}^{-1} \mathbf{U}_{\prec j}], \mathbf{D}_{jj} \mathbf{U}_{\prec j \succ}^{-1} \right), \\ \eta_j | \mathbf{L}_{\prec j}], \mathbf{D}_{jj} &\sim \mathcal{N} \left(m_j + \mathbf{L}_{\prec j}]^{\top} \mathbf{m}_{\prec j \succ}, \mathbf{D}_{jj} / a_{\mu} \right) \end{aligned}$$

and $a_j^{\mathcal{D}} = a_{\Omega} + |\text{pa}_{\mathcal{D}}(j)| - q + 1$.

3.2 Prior on DAG structures

Let \mathcal{S}_q be the space of all DAGs on q nodes. For a given DAG $\mathcal{D} = (V, E) \in \mathcal{S}_q$, let $\mathbf{S}^{\mathcal{D}}$ be the 0-1 *adjacency matrix* of its skeleton, that is the underlying undirected graph obtained after removing the orientation of all its edges. Accordingly, for each (u, v) -element in $\mathbf{S}^{\mathcal{D}}$, $\mathbf{S}_{u,v}^{\mathcal{D}} = 1$ if and only if $(u, v) \in E$ or $(v, u) \in E$, and zero otherwise. Conditionally on a prior probability of inclusion $\pi \in (0, 1)$ we assume $\mathbf{S}_{u,v}^{\mathcal{D}} | \pi \stackrel{\text{iid}}{\sim} \text{Ber}(\pi)$ for each $u > v$. Therefore,

$$p(\mathbf{S}^{\mathcal{D}} | \pi) = \pi^{|\mathbf{S}^{\mathcal{D}}|} (1 - \pi)^{\frac{q(q-1)}{2} - |\mathbf{S}^{\mathcal{D}}|}, \quad (15)$$

where $|\mathbf{S}^{\mathcal{D}}|$ is the number of edges in \mathcal{D} (equivalently in its skeleton) and $q(q-1)/2$ corresponds to the maximum number of edges in a DAG on q nodes.

We then proceed hierarchically by assigning $\pi \sim \text{Beta}(a, b)$. Integrating out π , the resulting prior on $\mathbf{S}^{\mathcal{D}}$ is

$$p(\mathbf{S}^{\mathcal{D}}) = \frac{\Gamma(|\mathbf{S}^{\mathcal{D}}| + a) \Gamma \left(\frac{q(q-1)}{2} - |\mathbf{S}^{\mathcal{D}}| + b \right)}{\Gamma \left(\frac{q(q-1)}{2} + a + b \right)} \cdot \frac{\Gamma(a + b)}{\Gamma(a) \Gamma(b)},$$

A similar prior was introduced by Scott & Berger [34] for variable selection in linear models, where it was also shown to account for multiplicity correction. Finally, we set

$$p(\mathcal{D}) \propto p(\mathbf{S}^{\mathcal{D}}), \quad \mathcal{D} \in \mathcal{S}_q. \quad (16)$$

Hyperparameters a and b can be chosen to reflect a prior knowledge of sparsity in the graph, if available; in the next section we fix for instance $a = 1$, $b = (2q - 2)/3$, which is consistent with an expected prior probability of edge inclusion smaller than 0.5; see also Peters & Bühlmann [30]. The default choice $a = b = 1$, which corresponds to $\pi \sim \text{Unif}(0, 1)$, can be instead adopted in the absence of substantive prior information.

Finally, the prior on the precision parameter is taken to be $\alpha_0 \sim \text{Gamma}(c, d)$. Hyperparameters $c, d > 0$ control the prior number of clusters [11]. A sensitivity analysis on a grid of values for c and d led to the choice (hereafter employed) $c = 3, d = 1$, which results in a moderate expected number of groups, and a 90% approximate prior credible interval $1 < \alpha_0 < 6$; see also Murugiah & Sweeting [26] for empirical approaches driving the choice of c and d .

4 Posterior inference: clustering, structural learning and causal effects

We implement an MCMC algorithm to sample from the posterior distribution of the DP mixture model (11). Our proposal relies on a *slice sampler* [39] which is based on the number of explicitly represented mixture components and maintains the structure of a blocked Gibbs sampler. Full details are provided in the Supplementary material.

The output of our MCMC scheme is a collection of S draws approximatively sampled from the (augmented) posterior of $(\boldsymbol{\xi}, \boldsymbol{\theta}^*)$ where $\boldsymbol{\theta}^*$ is the triple $(\boldsymbol{\mu}^*, \boldsymbol{\Omega}^*, \mathcal{D}^*)$. Specifically, for each MCMC iteration $t = 1, \dots, S$ our algorithm returns the n -dimensional vector of individual allocations $\boldsymbol{\xi}^{(t)} = (\xi_1^{(t)}, \dots, \xi_n^{(t)})$, with $\xi_i^{(t)} \in \{1, \dots, K^{(t)}\}$ where $K^{(t)}$ is the number of distinct clusters, together with the collection of $K^{(t)}$ distinct cluster-specific parameters $\{\boldsymbol{\theta}_1^{(t)}, \dots, \boldsymbol{\theta}_{K^{(t)}}^{(t)}\}$. From the MCMC output we can construct an (n, n) posterior similarity matrix \mathbf{S} whose (i, i') -element represents the posterior probability that subjects i and i' belong to the same cluster, namely

$$\widehat{p}(\xi_i = \xi_{i'} \mid \mathbf{X}) = \frac{1}{S} \sum_{t=1}^S \mathbb{1} \left\{ \xi_i^{(t)} = \xi_{i'}^{(t)} \right\}. \quad (17)$$

The latter can be used to obtain an estimate $\widehat{\mathbf{c}}$ of the partition induced by the DP, e.g. by including subject i and i' in the same cluster whenever $\widehat{p}(\xi_i = \xi_{i'} \mid \mathbf{X})$ exceeds a given threshold, say 0.5, as we do in the simulation results of Section 5.

MCMC samples may also be used to provide subject-specific estimates of DAGs and parameters that are needed to estimate causal effects for each individual as set out in the motivations described in Section 1.1. To this end, we start by defining for each subject i and edge (u, v) , $u \neq v$, the posterior probability of edge inclusion

$$\hat{p}_i(u \rightarrow v | \mathbf{X}) = \frac{1}{S} \sum_{t=1}^S \mathbb{1} \left\{ (u, v) \in \mathcal{D}_{\xi_i^{(t)}}^{(t)} \right\}. \quad (18)$$

where, with a slight abuse of notation, $\mathbb{1} \{(u, v) \in \mathcal{D}\} = 1$ if \mathcal{D} contains the edge $u \rightarrow v$, and zero otherwise. A DAG estimate $\hat{\mathcal{D}}_i$ can be obtained by including only those edges $u \rightarrow v$ for which $\hat{p}_i(u \rightarrow v | \mathbf{X}) > w$. If $w = 0.5$ this results in the median probability DAG, which we adopt as a DAG point estimate throughout our simulation study.

Recall now the definition of causal effect γ_s as a function of the precision (inverse-covariance) matrix in Equation (4). A Bayesian model averaging (BMA) estimate of γ_s for individual i can be recovered from the MCMC output as $\hat{\gamma}_{s,i}$

$$\hat{\gamma}_{s,i} = \frac{1}{S} \sum_{t=1}^S \gamma_{s,i}^{(t)}, \quad (19)$$

where $\gamma_{s,i}^{(t)}$ is computed as in (10) by setting $\boldsymbol{\Sigma} = [\boldsymbol{\Omega}_{\xi_i}^{(t)}]^{-1}$.

5 Simulations

In this section we evaluate the performance of our method through simulation studies.

5.1 Settings

We consider settings with $q = 20$ nodes and $K = 2$ clusters while we vary the sample size $n_k \in \{50, 100, 200, 500\}$. In addition, cluster-specific parameters $\boldsymbol{\theta}_k = (\mathbf{D}_k, \mathbf{L}_k, \boldsymbol{\eta}_k, \mathcal{D}_k)$ are generated under two scenarios. In *Equal DAGs* (scenario) we randomly generate a sparse DAG \mathcal{D}_1 by fixing a probability of edge inclusion equal to 0.1 and set $\mathcal{D}_2 = \mathcal{D}_1$, which implies that the two DAG models are structurally equal; in *Different DAGs* (scenario) we instead generate \mathcal{D}_1 and \mathcal{D}_2 independently, so that \mathcal{D}_1 and \mathcal{D}_2 are different in general. DAG parameters $(\mathbf{D}_k, \mathbf{L}_k, \boldsymbol{\eta}_k)$ are generated independently across k by setting $\mathbf{D}_k = \mathbf{I}_q$, while uniformly sampling the non-zero elements of \mathbf{L}_k in $[-1, -0.1] \cup [0.1, 1]$; in addition, to evaluate the performance of our method in the cluster identification we sample the elements of each $\boldsymbol{\eta}_k$ in the interval $[-b, b]$, with $b \in \{1, 2, 5\}$. Intuitively, the difference in mean values implied by the increasing size of the interval $[-b, b]$ is expected to affect the ability of our method to separate the two groups. We then set $\mathbf{U} = \mathbf{I}_q$, $a_\mu = 1$, $\mathbf{m} = \mathbf{0}$, $a_\Omega = q$ in the Normal-DAG-Wishart prior. In doing so, the weight assigned to the prior is equivalent to the weight of one observed sample; see also Rodríguez et al.

[32] for a comparison. Furthermore, to favor sparsity, we fix $a = 1$, $b = (2q - 2)/3$ in the Beta prior on π leading to the prior on DAGs (16). From further simulation experiments not reported for brevity it also appeared that results are quite insensitive to these hyperparameter choices, especially for large sample sizes. Under each scenario we then perform $N = 20$ simulations. Our MCMC scheme is implemented for a number of MCMC iteration $S = 25000$, after having assessed its convergence through some pilot runs.

5.2 Clustering

We first evaluate the performance of our method with regard to cluster allocation. To this end, we compare the true partition \mathbf{c} with the estimated partition $\widehat{\mathbf{c}}$ by means of the Binder Loss (BL) [4] and the Variation of Information (VI) [24]. The two metrics, normalized in $[0, 1]$ are respectively defined as

$$\begin{aligned} \text{BL}(\mathbf{c}, \widehat{\mathbf{c}}) &= \frac{2}{n(n-1)} \sum_{i < j} \{ \mathbb{1}(c_i = c_j) \mathbb{1}(\widehat{c}_i \neq \widehat{c}_j) + \mathbb{1}(c_i \neq c_j) \mathbb{1}(\widehat{c}_i = \widehat{c}_j) \}, \\ \text{VI}(\mathbf{c}, \widehat{\mathbf{c}}) &= \frac{1}{\log(n)} \{ H(\mathbf{c}) + H(\widehat{\mathbf{c}}) - 2I(\mathbf{c}, \widehat{\mathbf{c}}) \}, \end{aligned}$$

with $H(\mathbf{c}) = -\sum_{k=1}^K p(k) \log p(k)$ and $I(\mathbf{c}, \widehat{\mathbf{c}}) = \sum_{k=1}^K \sum_{h=1}^H p(k, h) \log \{p(k, h)/p(k)p(h)\}$ representing the entropy associated to clustering \mathbf{c} , and the mutual information between the two clusterings $\mathbf{c}, \widehat{\mathbf{c}}$, where $p(k) = \sum_i \mathbb{1}(c_i = k)/n$ and $p(k, h) = \sum_i \mathbb{1}(c_i = k, \widehat{c}_i = h)/n$; see also Meilă [24]. Intuitively, lower values of the two indexes correspond to better performances in the clustering allocation. We compute BL and VI under each simulated dataset and scenario. Results are summarized in the plots of Figure 1. Each sequence of points joined by a dotted line represents the average values (w.r.t. the $N = 20$ simulations) of an index computed for increasing sample sizes n_k and one value of b (with increasing values of b from dark to light grey). It appears that the performance of the method improves as n_k grows under each scenario both in terms of BL and VI. Moreover, higher values of b make cluster identification easier even for moderate sample sizes, e.g. $n_k = 50$. In addition, the clustering performance is better under *Different DAGs* scenario which corresponds to settings with DAGs generated independently and therefore also “structurally” different.

5.3 Structural learning

We now evaluate the performance of our method in learning the graph structures. To this end, under each simulation, we measure the Structural Hamming Distance (SHD) between each (individual) estimated DAG $\widehat{\mathcal{D}}_i$, $i = 1, \dots, n$ and the corresponding true DAG. SHD corresponds to the number of edge insertions, deletions or flips needed to transform the estimated DAG into the true one; accordingly, lower values of SHD corresponds to better performances.

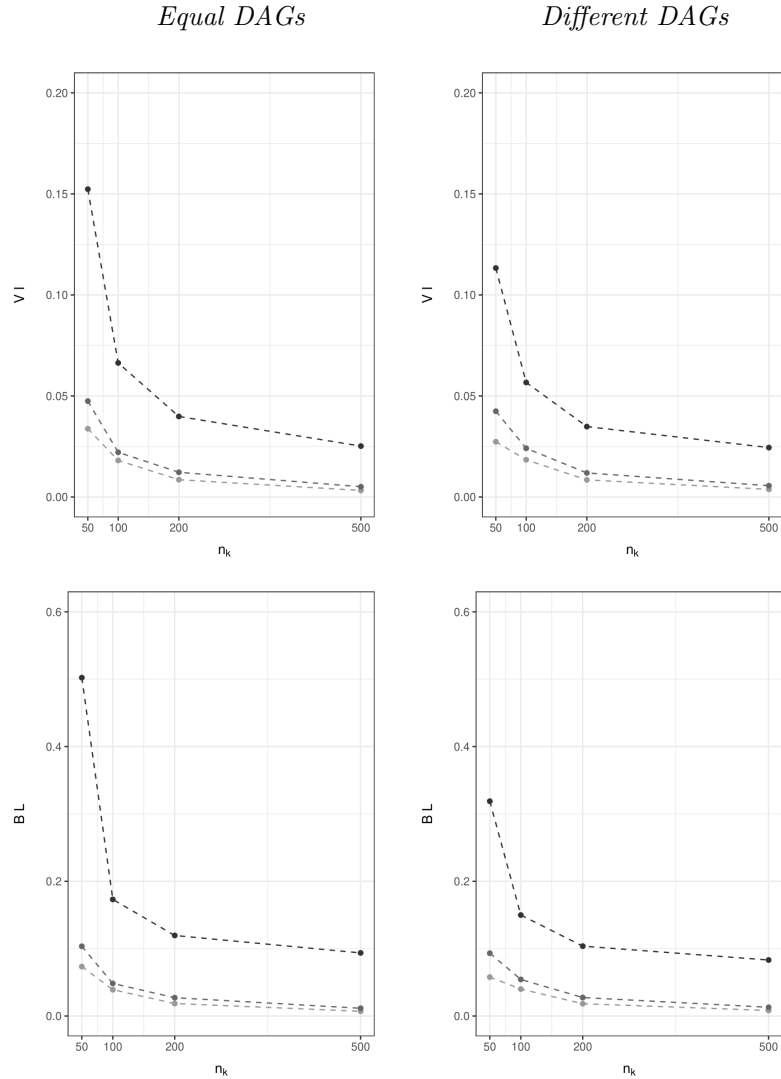


Figure 1: Simulations. Average (w.r.t. 20 simulations) Variation of Information (VI) and Binder Loss (BL) index under *Equal DAGs* and *Different DAGs* scenarios, for increasing sample sizes $n_k \in \{50, 100, 200, 500\}$. Dark, middle and light grey dots correspond to values of $b \in \{1, 2, 5\}$ respectively.

For comparison purposes, we also include two alternative, yet opposed, learning strategies which are not based on DP mixture models. The first one corresponds to an oracle setting wherein the true two-group clustering is known beforehand. We call this benchmark *Two-group oracle*. The second instead wrongly assumes that all observations are conditionally iid from the same one-component model, and we name it *One-group naive*. Both benchmarks try to evaluate differential performance in structural learning: the former assesses the gain afforded by removing imperfect knowledge on clustering; the latter instead captures decay due to naively neglecting heterogeneity. In both benchmark strategies, while not running a DP mixture model, we use the same specifications for the prior on DAG- and parameter space.

Results are summarized in the plots of Figure 2. Each box-plot represents the distribution of SHD, averaged with respect to individuals belonging to the same true cluster, for one strategy under comparison and scenarios *Equal DAGs* and *Different DAGs* with increasing values of $b \in \{1, 2, 5\}$ (from left to right panels) and group sample size $n_k \in \{50, 100, 200, 500\}$. It appears that *One-group naive* performs worse w.r.t. the other two methods under both scenarios. In particular its performance worsens as n_k increases and for larger values of b , because under both circumstances the two clusters become better separated. Reassuringly, *Two-group oracle* performs only slightly better than our *DP mixture* method even in the setting $b = 1$, where cluster identification is more difficult, with results nearly indistinguishable for $n_k \in \{200, 500\}$. In addition, both methods improve their performance as n_k grows.

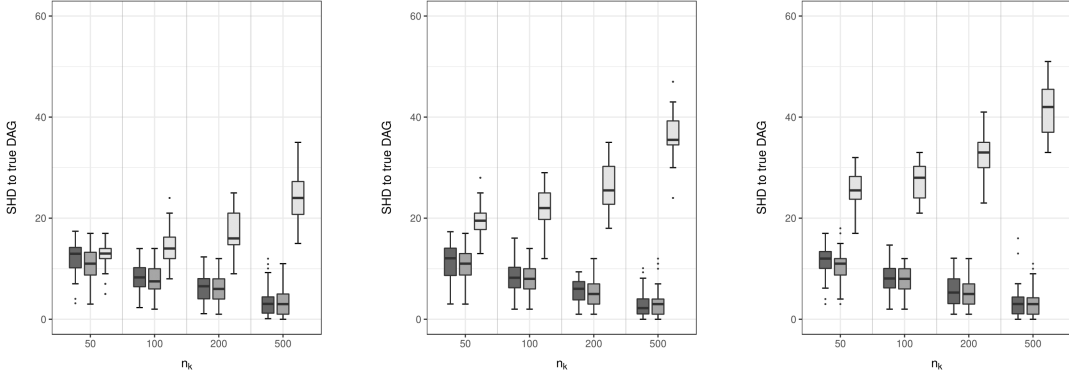
5.4 Causal effect estimation

We finally consider causal effect estimation. Under each scenario, we compare the collection of subject-specific BMA causal effect estimates $\hat{\gamma}_{s,i}$, $i = 1, \dots, n$, $s = 1, \dots, q$, in Equation (19) with the corresponding true causal effects $\gamma_{s,i}$ by means of the absolute-value distance

$$d_{s,i} = |\hat{\gamma}_{s,i} - \gamma_{s,i}|.$$

The distribution of $d_{s,i}$ across subjects and simulated datasets is summarized through the average distance whose percentage values, computed under each scenario, are reported in Tables 1 and 2; the two tables refer to scenarios *Equal DAGs* and *Different DAGs* respectively. For comparisons, we also compute the same collection of causal effect estimates under *Two-group oracle*. It appears that, while both methods improve their performances as b and n_k grows, *DP mixtures* performs only slightly worse than *Two-group oracle*. In addition, such differences are more evident under scenarios with moderate sample size n_k and smaller values of b , e.g. $b = 1$, where indeed cluster allocation was also more difficult.

Equal DAGs



Different DAGs

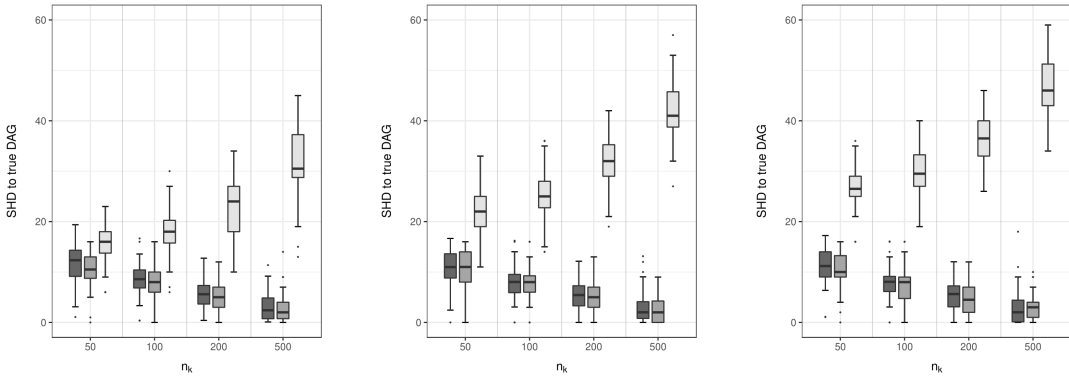


Figure 2: Simulations. Structural Hamming Distance (SHD) between estimated and true DAGs under *Equal DAGs* and *Different DAGs* scenarios, for increasing sample sizes $n_k \in \{50, 100, 200, 500\}$ and increasing values of $b \in \{1, 2, 5\}$ (from left to right panels). Dark, medium and light grey box-plots correspond to *DP mixture*, *Two-group oracle* and *One-group naive* strategies respectively.

	n_k	50	100	200	500
$b = 5$	<i>DP mixture</i>	3.18	2.75	2.15	1.60
	<i>Two-group oracle</i>	2.72	2.56	2.00	1.47
$b = 2$	<i>DP mixture</i>	3.41	2.90	2.25	1.72
	<i>Two-group oracle</i>	2.80	2.70	2.05	1.63
$b = 1$	<i>DP mixture</i>	3.65	2.91	2.25	1.63
	<i>Two-group oracle</i>	2.90	2.56	2.04	1.41

Table 1: Simulations. *Equal DAGs* scenario. Average absolute-value distance (computed across simulations and subjects) between estimated and true subject-specific causal effect. Results reported for values of $n_k \in \{50, 100, 200, 500\}$ and $b = \{1, 2, 5\}$.

	n_k	50	100	200	500
$b = 5$	<i>DP mixture</i>	3.44	2.91	2.66	1.70
	<i>Two-group oracle</i>	3.10	2.63	2.60	1.67
$b = 2$	<i>DP mixture</i>	3.83	2.97	2.64	1.80
	<i>Two-group oracle</i>	3.18	2.66	2.60	1.64
$b = 1$	<i>DP mixture</i>	4.19	3.06	2.74	1.90
	<i>Two-group oracle</i>	3.00	2.64	2.59	1.79

Table 2: Simulations. *Different DAGs* scenario. Average absolute-value distance (computed across simulations and subjects) between estimated and true subject-specific causal effect. Results reported for values of $n_k \in \{50, 100, 200, 500\}$ and $b = \{1, 2, 5\}$.

6 Analysis of gene expressions from GBM patients

In this section we apply our methodology to the gene expression dataset of patients affected by glioblastoma (GBM) mentioned in the Introduction. The dataset (available within our Supplementary material) includes gene expression measurements relative to the $q = 20$ genes involved in the $\text{TGF}\beta$ pathway. Observations are collected on $n = 70$ patients affected by GBM and include long, intermediate and short time survivors. We recall that GBM is widely heterogeneous at the cellular, genomic and transcriptional levels, a feature which is supposedly due to the presence of a subpopulation of cancer stem cells (CSC). Because of their role in the regulation of tumor cells, $\text{TGF}\beta$ proteins represent natural response variables for the causal effect analysis here considered. By contrast, each gene involved in the pathway may represent a suitable target of intervention whose inhibition can induce the desired regulation-effect of $\text{TGF}\beta$ proteins ($\text{TGF}\beta 1$, $\text{TGF}\beta 2$, $\text{TGF}\beta 3$) and allied receptors $\text{TGF}\beta\text{R}1$, $\text{TGF}\beta\text{R}2$.

We implement the proposed model by running our MCMC scheme for $S = 120000$ iterations, which includes a burn-in period of 20000 runs. We fix hyper-parameters $c = 3$, $d = 1$ in the Gamma prior on the precision parameter α_0 , which is consistent with a moderate expected number of clusters K . In addition, we set $\mathbf{U} = \mathbf{I}_q$, $a_\mu = 1$, $\mathbf{m} = \mathbf{0}$, $a_\Omega = q$ in the Normal-DAG-Wishart prior as in the simulation settings of Section 5.1. With regard to the Beta prior on the probability of edge inclusion π we instead fix $a = 1$, $b = 10$, which reflects a moderate degree of sparsity in the pathway. To assess the convergence of our algorithm we also run independent MCMC chains with results suggesting a highly satisfactory agreement in terms of clustering, graph structure learning and causal effect estimation; see also the Supplementary material for further details.

Based on the MCMC output we first produce the (n, n) similarity matrix based on the posterior probabilities (17) computed for each pair of subjects (i, i') , $i \neq i'$. In particular, fixing a threshold for clustering inclusion equal to 0.5, we obtain a partition with three groups of size $n_1 = 55$, $n_2 = 13$, $n_3 = 2$. For ease of interpretation we numbered subjects in cluster 1 from 1 to 55, followed by those in cluster 2 from 56 to 68, while those in cluster 3 have numbers 69 and 70. Results are summarized in the heat map of Figure 3 where the axes report the ordered subjects. A few subjects in cluster 1, notably 10, 22, 23, 32 and 35, appear to be borderline in the sense that they barely qualify for membership. For instance, it appears that subject 23 belongs to cluster 1 with probability around 70% and to cluster 2 with probability 30%; as a consequence membership in this case is more uncertain. The three groups are associated with levels in the expression of proteins which can vary appreciably; this is particularly true for $\text{TGF}\beta 1$ and $\text{TGF}\beta\text{R}2$, as in Figure 4. In particular, cluster 1 appears to be up-regulated across the entire $\text{TGF}\beta$ family, suggesting stronger progression of the disease [5]. Accordingly one should also expect differences in the regulation of $\text{TGF}\beta$ proteins which is induced by gene modifications as in our causal-effect framework.

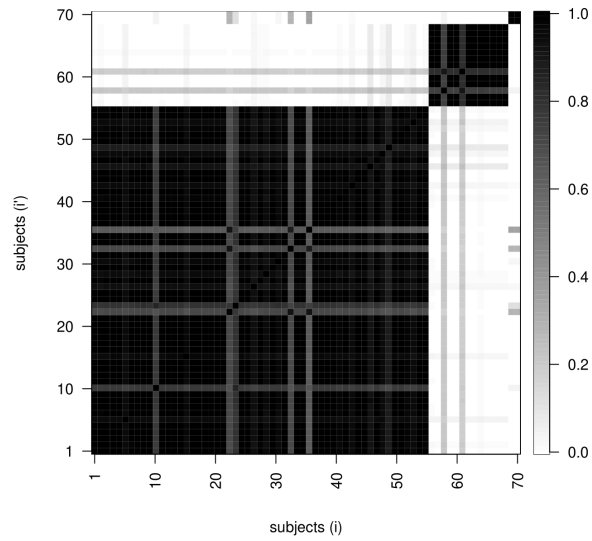


Figure 3: GBM data. Posterior similarity matrix. Subjects arranged by cluster membership.

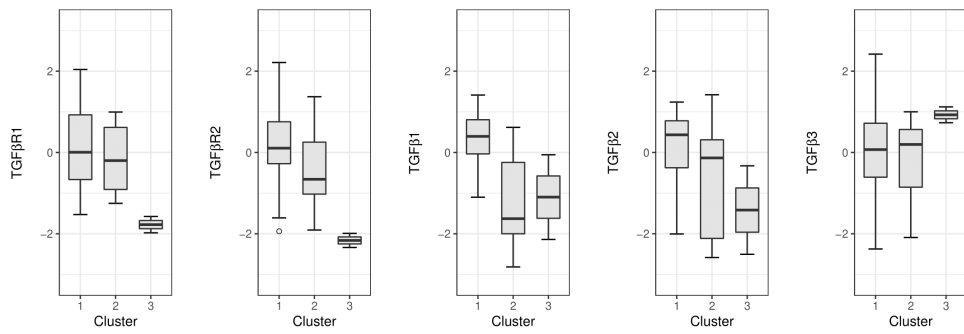


Figure 4: GBM data. Box-plots of TGF β proteins' level for each of the three estimated clusters.

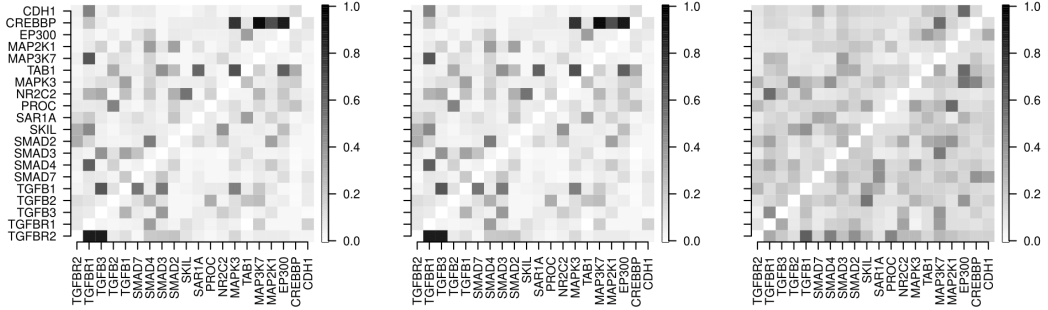


Figure 5: GBM data. Heat maps of posterior edge inclusion probabilities for three subject-specific graphs. Left and center maps are for two subjects in cluster 1; right map for a subject in cluster 2

We now focus on graph structure learning. Specifically, we construct for each subject $i = 1, \dots, n$ a (q, q) matrix collecting the posterior inclusion probabilities of each (directed) edge (u, v) , $u \neq v$. Results for three randomly chosen subjects, whose membership is estimated to be cluster 1 for two subjects and cluster 2 for the remaining one, are reported in Figure 5. The three heat maps reveal an appreciable degree of sparsity in each of the three underlying DAG structures. It is also apparent that the two subjects belonging to the same cluster share most of the basic structure, although with some slight differences in the strength of gene-dependencies encoded in posterior probabilities of edge inclusion. More interestingly, the dependence structure for the third subject is substantially different from that of the remaining two.

Using Equation (19), we can provide a subject-specific BMA estimate of the causal effect on each of the responses $TGF\beta 1$, $TGF\beta 2$, $TGF\beta 3$, $TGF\beta R1$, $TGF\beta R2$ following an intervention on any other of the 20 genes s involved in the pathway leading to the collection $\gamma_{i,s}$, $s = 1, \dots, 20$ for each subject $i = 1, \dots, 70$. Results are summarized in the heat maps of Figure 6 where each plot refers to one of the five response variables. The pattern already observed in Figure 3 is also apparent. Subjects assigned to the same cluster reveal broadly similar causal effect estimates, with some notable exceptions for a few individuals within the first group. For instance subject 23 whose membership was more uncertain (70% for cluster 1 and 30% for cluster 2) has a BMA estimate of some causal effects which are more similar to those in cluster 2 rather than his neighbors in cluster 1; see for instance panel $TGF\beta 1$ in Figure 6 along row $TAB1$ or panel $TGF\beta R1$ along $SMAD2$ in the same figure. Similar comments hold for subject 61 whose pattern differs appreciably from his neighbors in several panels and for most genes.

More interestingly, the effect of an intervention on the same gene may significantly vary across subjects. This happens for instance with regard to most $SMAD$ proteins which exhibit a (positive) causal effect w.r.t. $TGF\beta$ proteins only relative to individuals assigned to the first cluster. Notably, proteins belonging to the $SMAD$ family have been shown to play a crucial

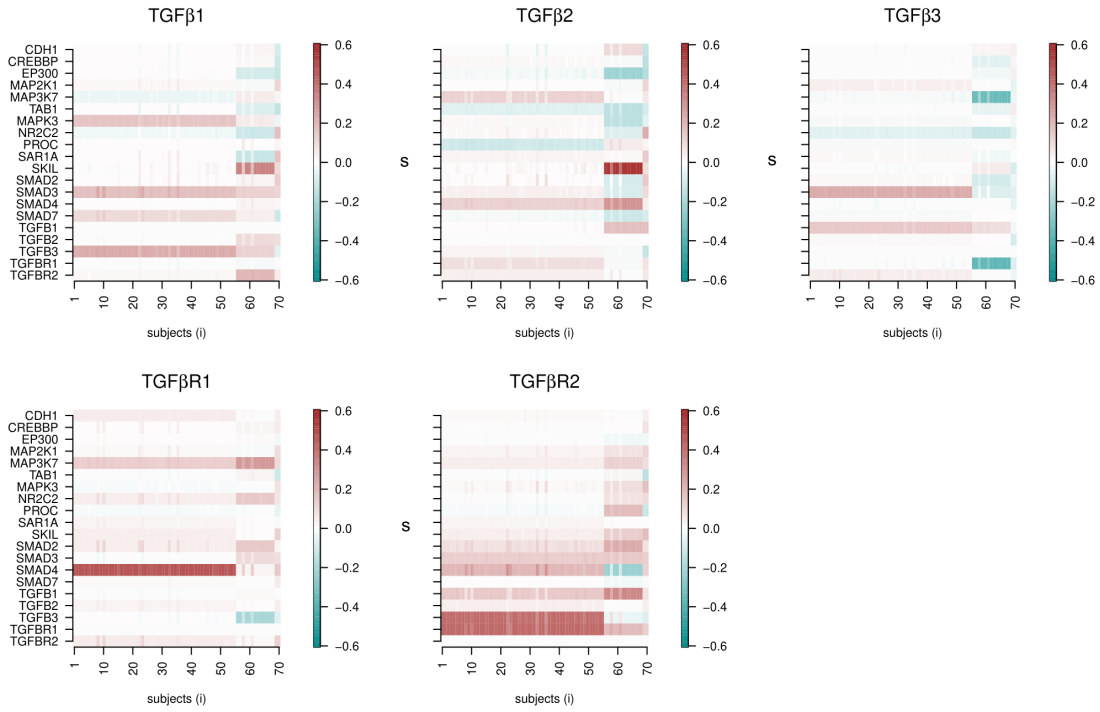


Figure 6: GBM data. Heat maps of causal effects on responses $TGF\beta_1$, $TGF\beta_2$, $TGF\beta_3$, $TGF\beta R1$, $TGF\beta R2$, following an intervention on one target gene s among the twenty involved in the $TGF\beta$ pathway. Subjects arranged by cluster membership.

role in cell proliferation, since they act as mediators of the signals initiated by $TGF\beta$ cytokines; see for instance Han et al. [18]. By converse, other genes, such as NR2C2 (nuclear hormone receptor family), are associated to non-null (negative) causal effects relative to subjects within the second cluster.

From a personalized therapy perspective, one can therefore argue that regulation of $TGF\beta$ proteins might be induced by gene modifications that should be selected at subject-specific level. In other words, one gene therapy aiming at $TGF\beta$ regulation through intervention of genes in the pathway, can result in heterogeneous effects, and corresponding levels of efficacy, across different subjects. Comparisons based on the alternative *One-group naive* strategy (Section 5.3) are contained in the Supplementary material. In brief, our findings reveal that an approach which neglects population heterogeneity may produce misleading estimates of causal effects.

7 Discussion

In this paper we present a Bayesian framework to evaluate heterogeneous causal effects based on Directed Acyclic Graphs (DAGs). We model heterogeneity through an infinite mixture model

which accounts for structure and parameter uncertainty. The output of our methodology is a collection of subject-specific causal effects, each being a Bayesian model average of causal effects across DAGs. Because of the discreteness of the process governing the generation of the individual parameters, a posterior distribution on the clustering structure of the units is also available.

Our analysis is based on a Dirichlet Process (DP) mixture of Gaussian DAG models. While more general Bayesian nonparametric models might be adopted, e.g. Müller & Mitra [25], and Barrios et al. [2], we believe that the main content of our contribution, namely causal inference under heterogeneity based on DAGs, is best captured by the current DP mixture model because of its popularity, interpretability and simplicity of implementation.

Gene expression levels are known to be affected by genetic, environmental, demographic, and other technical factors. This means that, in addition to the measured variables, there will typically be sources of heterogeneity which are hidden or latent, and failing to incorporate these sources may have detrimental effects on the study [22]. In our model we do not consider latent variables because this would add a significant layer of complexity both at the stage of learning the underlying causal structure [14] and of identifying causal effects [37].

The type of interventions we have considered may be called *perfect*, meaning that they eliminate dependencies between targeted variables and their direct causes; the identifiability of causal DAGs under perfect interventions was characterized by Hauser & Bühlmann [19]. More recently the broader notion of *general* intervention has been introduced, which may modify the dependencies between targeted variables and their causes without eliminating them; see Yang et al. [42].

Acknowledgments This research was partially supported by UCSC (D1 and 2019-D.3.2 research grants). We thank Raffaele Argiento for useful discussions on the slice sampler.

SUPPLEMENTARY MATERIAL

The file **supplementary_material.pdf** provides supplemental information to our paper, which is organized into three sections. Section 1 contains a detailed description of the elicitation procedure leading to compatible priors for DAG-model parameters based on Normal-DAG-Wishart distributions. Section 2 describes our MCMC scheme for posterior inference on DAG structures, cluster allocation parameters and causal effects. Finally, Section 3 provides convergence diagnostics relative to the application on GBM data, and comparisons with a naive strategy which does not account for heterogeneity.

References

- [1] ATHEY, S. & IMBENS, G. (2016). Recursive Partitioning for Heterogeneous Causal Effects 113 7353–7360.
- [2] BARRIOS, E., LIJOI, A., NIETO-BARAJAS, L. E. & PRÜNSTER, I. (2013). Modeling with Normalized Random Measure Mixture Models. *Statistical Science* 28 313–334.
- [3] BÜHLMANN, P. (2020). Invariance, Causality and Robustness. *Statistical Science* 35 404–426.
- [4] BINDER, D. A. (1978). Bayesian Cluster Analysis. *Biometrika* 65 31–38.
- [5] BIRCH, J. L., COULL, B. J., SPENDER, L. C., WATT, C., WILLISON, A., SYED, N., CHALMERS, A. J., HOSSAIN-IBRAHIM, M. K. & INMAN, G. J. (2020). Multifaceted Transforming Growth Factor-Beta (TGF β) Signalling in Glioblastoma. *Cell Signalling* 72.
- [6] CAO, X., KHARE, K. & GHOSH, M. (2019). Posterior Graph Selection and Estimation Consistency for High-Dimensional Bayesian DAG Models. *The Annals of Statistics* 47 319–348.
- [7] CASTELLETTI, F. & CONSONNI, G. (2021). Bayesian Causal Inference in Probit Graphical Models. *Bayesian Analysis* 1 – 25.
- [8] CASTELLETTI, F. & CONSONNI, G. (2021). Bayesian Inference of Causal Effects from Observational Data in Gaussian Graphical Models. *Biometrics* 77 136–149.
- [9] CASTELLETTI, F., LA ROCCA, L., PELUSO, S., STINGO, F. C. & CONSONNI, G. (2020). Bayesian Learning of Multiple Directed Networks from Observational Data. *Statistics in Medicine* 39 4745–4766.
- [10] CREMASCHI, A., ARGIENTO, R., SHOEMAKER, K., PETERSON, C. & VANNUCCI, M. (2019). Hierarchical Normalized Completely Random Measures for Robust Graphical Modeling. *Bayesian Analysis* 14 1271–1301.
- [11] ESCOBAR, M. D. & WEST, M. (1995). Bayesian Density Estimation and Inference Using Mixtures. *Journal of the American Statistical Association* 90 577–588.
- [12] FINEGOLD, M. & DRTON, M. (2011). Robust Graphical Modeling of Gene Networks Using Classical and Alternative t -Distributions. *The Annals of Applied Statistics* 5 1057–1080.
- [13] FINEGOLD, M. & DRTON, M. (2014). Robust Bayesian Graphical Modeling Using Dirichlet t -Distributions. *Bayesian Analysis* 9 521–550.

[14] FROT, B., JOSTINS, L. & MCVEAN, G. (2019). Graphical Model Selection for Gaussian Conditional Random Fields in the Presence of Latent Variables. *Journal of the American Statistical Association* 114 723–734.

[15] GEIGER, D. & HECKERMAN, D. (2002). Parameter Priors for Directed Acyclic Graphical Models and the Characterization of Several Probability Distributions. *The Annals of Statistics* 30 1412–1440.

[16] GODSILL, S. J. (2012). On the Relationship Between Markov Chain Monte Carlo Methods for Model Uncertainty. *Journal of Computational and Graphical Statistics* 10 230–248.

[17] HAHN, P. R., MURRAY, J. S. & CARVALHO, C. M. (2020). Bayesian Regression Tree Models for Causal Inference: Regularization, Confounding, and Heterogeneous Effects (with Discussion). *Bayesian Analysis* 15 965–1056.

[18] HAN, J., ALVAREZ-BRECKENRIDGE, C., WANG, Q. E. & YU, J. (2015). TGF- β Signaling and its Targeting for Glioma Treatment. *American Journal of Cancer Research* 5 945–955.

[19] HAUSER, A. & BÜHLMANN, P. (2012). Characterization and Greedy Learning of Interventional Markov Equivalence Classes of Directed Acyclic Graphs. *Journal of Machine Learning Research* 13 2409–2464.

[20] LAURITZEN, S. L. (1996). *Graphical Models*. Oxford University Press.

[21] LEE, K., BARGAGLI-STOFFI, F. J. & DOMINICI, F. (2020). Causal Rule Ensemble: Interpretable Inference of Heterogeneous Treatment Effects. ArXiv preprint, 2009.09036.

[22] LEEK, J. T. & STOREY, J. (2007). Capturing Heterogeneity in Gene Expression Studies by Surrogate Variable Analysis. *PLoS Genetics* 3 1724–1735.

[23] MAATHUIS, M. & NANDY, P. (2016). A Review of Some Recent Advances in Causal Inference. In P. Bühlmann, P. Drineas, M. Kane & M. van der Laan, eds., *Handbook of Big Data*. Chapman and Hall/CRC, 387–408.

[24] MEILÄ, M. (2007). Comparing Clusterings - an Information Based Distance. *Journal of Multivariate Analysis* 98 873–895.

[25] MÜLLER, P. & MITRA, R. (2013). Bayesian Nonparametric Inference – Why and How. *Bayesian Analysis* 8 269–302.

[26] MURUGIAH, S. & SWEETING, T. (2012). Selecting the Precision Parameter Prior in Dirichlet Process Mixture Models. *Journal of Statistical Planning and Inference* 142 1947–1959.

[27] NI, Y., STINGO, F. C. & BALADANDAYUTHAPANI, V. (2017). Sparse Multi-Dimensional Graphical Models: A Unified Bayesian Framework. *Journal of the American Statistical Association* 112 779–793.

[28] PARSONS, D. W., JONES, S., ZHANG, X., LIN, J. C.-H., LEARY, R. J., ANGENENDT, P., MANKOO, P., CARTER, H., SIU, I.-M., GALLIA, G. L., OLIVI, A., MCLENDON, R., RASHEED, B. A., KEIR, S., NIKOLSKAYA, T., NIKOLSKY, Y., BUSAM, D. A., TEKLEAB, H., DIAZ, L. A., HARTIGAN, J., SMITH, D. R., STRAUSBERG, R. L., MARIE, S. K. N., SHINJO, S. M. O., YAN, H., RIGGINS, G. J., BIGNER, D. D., KARCHIN, R., PAPADOPOULOS, N., PARMIGIANI, G., VOGELSTEIN, B., VELCULESCU, V. E. & KINZLER, K. W. (2008). An Integrated Genomic Analysis of Human Glioblastoma Multiforme 321 1807–1812.

[29] PEARL, J. (2000). *Causality: Models, Reasoning, and Inference*. Cambridge University Press, Cambridge.

[30] PETERS, J. & BÜHLMANN, P. (2014). Identifiability of Gaussian Structural Equation Models with Equal Error Variances. *Biometrika* 101 219–228.

[31] PETERSON, C., STINGO, F. C. & VANNUCCI, M. (2015). Bayesian Inference of Multiple Gaussian Graphical Models. *Journal of the American Statistical Association* 110 159–174.

[32] RODRÍGUEZ, A., LENKOSKI, A. & DOBRA, A. (2011). Sparse Covariance Estimation in Heterogeneous Samples. *Electronic Journal of Statistics* 5 981–1014.

[33] RUBIN, D. B. (1974). Estimating Causal Effects of Treatments in Randomized and Non-randomized Studies. *Journal of Educational Psychology* 66 688–701.

[34] SCOTT, J. G. & BERGER, J. O. (2010). Bayes and Empirical-Bayes Multiplicity Adjustment in the Variable-Selection Problem. *The Annals of Statistics* 38 2587–2619.

[35] SHEN, R., OLSHEN, A. B. & LADANYI, M. (2009). Integrative Clustering of Multiple Genomic Data Types Using a Joint Latent Variable Model with Application to Breast and Lung Cancer Subtype Analysis. *Bioinformatics* 25 2906–2912.

[36] SHPITSER, I. & SHERMAN, E. (2018). Identification of Personalized Effects Associated with Causal Pathways. In *Proceedings of the 34th Annual Conference on Uncertainty in Artificial Intelligence*, UAI-18.

[37] SHPITSER, I. & TCHETGEN TCHETGEN, E. (2016). Causal Inference with a Graphical Hierarchy of Interventions. *The Annals of Statistics* 44 2433–2466.

- [38] WAGER, S. & ATHEY, S. (2018). Estimation and Inference of Heterogeneous Treatment Effects using Random Forests. *Journal of the American Statistical Association* 113 1228–1242.
- [39] WALKER, S. G. (2007). Sampling the Dirichlet Mixture Model with Slices. *Communications in Statistics - Simulation and Computation* 36 45–54.
- [40] WILKERSON, M. D. & HAYES, D. N. (2010). ConsensusClusterPlus: a Class Discovery Tool with Confidence Assessments and Item Tracking. *Bioinformatics* 26 1572–1573.
- [41] WITTE, J., HENCKEL, L., MAATHUIS, M. H. & DIDELEZ, V. (2020). On Efficient Adjustment in Causal Graphs. *Journal of Machine Learning Research* 21 1–45.
- [42] YANG, K., KATCOFF, A. & UHLER, C. (2018). Characterizing and Learning Equivalence Classes of Causal DAGs under Interventions. In J. Dy & A. Krause, eds., *Proceedings of the 35th International Conference on Machine Learning*, vol. 80 of *Proceedings of Machine Learning Research*. PMLR, 5541–5550.
- [43] ZHANG, W., LE, T. D., LIU, L., ZHOU, Z.-H. & LI, J. (2017). Mining Heterogeneous Causal Effects for Personalized Cancer Treatment. *Bioinformatics* 33 2372–2378.

Supplementary material for Bayesian graphical modelling for heterogeneous causal effects

This supplementary material comprises three sections. Section 1 contains a detailed description of the elicitation procedure leading to compatible priors for DAG-model parameters based on Normal-DAG-Wishart distributions. Section 2 describes our MCMC scheme for posterior inference on DAG structures, cluster allocation parameters and causal effects. Finally, Section 3 provides convergence diagnostics relative to our application to GBM data, and comparisons with an alternative strategy which does not account for heterogeneity.

1 Prior elicitation for DAG parameters

For the collection of random variables (X_1, \dots, X_q) consider the Gaussian DAG model

$$X_1, \dots, X_q | \boldsymbol{\mu}, \boldsymbol{\Omega}, \mathcal{D} \sim \mathcal{N}_q(\boldsymbol{\mu}, \boldsymbol{\Omega}^{-1}), \quad (1)$$

where $\boldsymbol{\mu} \in \mathbb{R}^q$ and $\boldsymbol{\Omega} \in \mathcal{P}_{\mathcal{D}}$, the space of all s.p.d. precision matrices Markov w.r.t. DAG \mathcal{D} . To assign a prior on $(\boldsymbol{\mu}, \boldsymbol{\Omega})$ we follow the procedure of Geiger & Heckerman [3] (G&H). This constructive method assumes some regularity conditions on the likelihood (*complete model equivalence, regularity, likelihood modularity*) which are satisfied by any Gaussian model. Starting from representation (7) in our paper for the joint density, the construction of the prior is based on two assumptions. The first one (*prior modularity*) states that, given two distinct DAG models with the *same* set of parents for vertex j , the prior for the node-parameter $\boldsymbol{\theta}_j$ must be the same under both models, namely

$$p(\boldsymbol{\theta}_j | \mathcal{D}_h) = p(\boldsymbol{\theta}_j | \mathcal{D}_k)$$

for any pair of distinct DAGs \mathcal{D}_h and \mathcal{D}_k such that $\text{pa}_{\mathcal{D}_h}(j) = \text{pa}_{\mathcal{D}_k}(j)$. The second one (*global parameter independence*) states that for every DAG model \mathcal{D} , the parameters $\{\boldsymbol{\theta}_j; j = 1, \dots, q\}$ should be *a priori* independent, that is

$$p(\boldsymbol{\theta} | \mathcal{D}) = \prod_{j=1}^q p(\boldsymbol{\theta}_j | \mathcal{D}).$$

If one follows the above path, it can be shown that the parameter priors across all DAG models are determined by a *unique* prior on the parameter of *any* of the (equivalent) *complete* DAGs; see Theorem 1 in G&H. Additionally all DAG-models within the same equivalence class will be scored equally (same marginal likelihood); see Theorem 3 in G&H. G&H (Section 4) also discuss the Gaussian case. For the benefit of the reader and for completeness of exposition we provide below the calculations leading to global parameter independence of the Cholesky parameters using our own notation and with some additional details.

1.1 Complete DAG case

Consider first the case in which \mathcal{D} is complete, so that $\boldsymbol{\Omega}$ is s.p.d. but otherwise *unconstrained*. A standard conjugate prior for $(\boldsymbol{\mu}, \boldsymbol{\Omega})$ is the Normal-Wishart distribution, $(\boldsymbol{\mu}, \boldsymbol{\Omega}) \sim \mathcal{NW}(a_\mu, \mathbf{m}, a_\Omega, \mathbf{U})$, with $a_\mu > 0$, $\mathbf{m} \in \mathbb{R}^q$, $a_\Omega > q - 1$ and \mathbf{U} s.p.d. Equivalently we can write

$$\boldsymbol{\mu} | \boldsymbol{\Omega} \sim \mathcal{N}_q(\mathbf{m}, (a_\mu \boldsymbol{\Omega})^{-1}), \quad \boldsymbol{\Omega} \sim \mathcal{W}_q(a_\Omega, \mathbf{U}),$$

where our notation for the Wishart means that the density is

$$p(\boldsymbol{\Omega}) \propto |\boldsymbol{\Omega}|^{\frac{a_\Omega - q - 1}{2}} \exp\left\{-\frac{1}{2}\text{tr}(\boldsymbol{\Omega}\mathbf{U})\right\}.$$

Assume for convenience a *parent ordering* of the nodes which numerically labels the q variables in such a way that $u > v$ whenever u is a parent of v . We introduce the re-parameterization $(\boldsymbol{\mu}, \boldsymbol{\Omega}) \mapsto (\boldsymbol{\eta}, \mathbf{L}, \mathbf{D})$, where \mathbf{L} is a (q, q) lower triangular matrix with all diagonal entries equal to one and \mathbf{D} a (q, q) diagonal matrix. In particular, given $\boldsymbol{\Sigma} = \boldsymbol{\Omega}^{-1}$, we have, for $j = 1, \dots, q$,

$$\mathbf{D}_{jj} = \boldsymbol{\Sigma}_{jj| \prec j \succ}, \quad \mathbf{L}_{\prec j]} = \boldsymbol{\Sigma}_{\prec j \succ}^{-1} \boldsymbol{\Sigma}_{\prec j]}, \quad \eta_j = \mu_j + \mathbf{L}_{\prec j]}^\top \boldsymbol{\mu}_{\prec j \succ}, \quad (2)$$

where $\boldsymbol{\Sigma}_{jj| \prec j \succ} = \boldsymbol{\Sigma}_{jj} - \boldsymbol{\Sigma}_{[j \succ} \boldsymbol{\Sigma}_{\prec j]}^{-1} \boldsymbol{\Sigma}_{\prec j]}$, and $\prec j] = \text{pa}_{\mathcal{D}}(j) \times j$, $[j \succ = j \times \text{pa}_{\mathcal{D}}(j)$, $\prec j \succ = \text{pa}_{\mathcal{D}}(j) \times \text{pa}_{\mathcal{D}}(j)$. Also notice that, because of the parent ordering on \mathcal{D} complete, we have $\text{pa}_{\mathcal{D}}(j) = \{j+1, \dots, q\}$ and $|\text{pa}_{\mathcal{D}}(j)| = q - j$, for each $j = 1, \dots, q$. We first consider the following Lemma.

Lemma 1.1. *Let $(\boldsymbol{\mu}, \boldsymbol{\Omega}) \sim \mathcal{NW}_q(a_\mu, \mathbf{m}, a_\Omega, \mathbf{U})$, $a_\mu > 0$, $\mathbf{m} \in \mathbb{R}^q$, $a_\Omega > q - 1$ and \mathbf{U} s.p.d. Consider the partition $\mathbf{x}^\top = (\mathbf{x}_{(1)}^\top \mathbf{x}_{(2)}^\top)$, where $\mathbf{x}_{(1)}$ is $(q_1, 1)$ and $\mathbf{x}_{(2)}$ is $(q_2, 1)$. Partition $\boldsymbol{\mu}, \boldsymbol{\Omega}$ and $\boldsymbol{\Sigma}$ accordingly as*

$$\boldsymbol{\mu} = \begin{pmatrix} \boldsymbol{\mu}_{(2)} \\ \boldsymbol{\mu}_{(1)} \end{pmatrix}, \quad \boldsymbol{\Omega} = \begin{pmatrix} \boldsymbol{\Omega}_{(2)(2)} & \boldsymbol{\Omega}_{(2)(1)} \\ \boldsymbol{\Omega}_{(1)(2)} & \boldsymbol{\Omega}_{(1)(1)} \end{pmatrix}, \quad \boldsymbol{\Sigma} = \begin{pmatrix} \boldsymbol{\Sigma}_{(2)(2)} & \boldsymbol{\Sigma}_{(2)(1)} \\ \boldsymbol{\Sigma}_{(1)(2)} & \boldsymbol{\Sigma}_{(1)(1)} \end{pmatrix}.$$

Then, $(\boldsymbol{\mu}_{(1)}, \boldsymbol{\Omega}_{(1)(1) | (2)}) \perp\!\!\!\perp (\boldsymbol{\gamma}_{(2)}, \boldsymbol{\Omega}_{(1)(2)}, \boldsymbol{\Omega}_{(2)(2)})$ where $\boldsymbol{\gamma}_{(2)} = \boldsymbol{\mu}_{(2)} + \boldsymbol{\Omega}_{(2)(2)}^{-1} \boldsymbol{\Omega}_{(2)(1)} \boldsymbol{\mu}_{(1)}$. Moreover

$$(\boldsymbol{\mu}_{(1)}, \boldsymbol{\Omega}_{(1)(1) | (2)}) \sim \mathcal{NW}_{q_1}(a_\mu, \mathbf{m}_{(1)}, a_\Omega - q_2, \mathbf{U}_{(1)(1)}).$$

Proof. See G&H, Theorem 5. \square

The following proposition establishes independence among node-parameters $(\mathbf{D}_{jj}, \mathbf{L}_{\prec j}], \eta_j)$, $j = 1, \dots, q$.

Proposition 1.1 (Global parameter independence). *Let $(\boldsymbol{\mu}, \boldsymbol{\Omega}) \sim \mathcal{NW}_q(a_\mu, \mathbf{m}, a_\Omega, \mathbf{U})$, $a_\mu > 0, \mathbf{m} \in \mathbb{R}^q, a_\Omega > q - 1$ and \mathbf{U} s.p.d. Consider the re-parameterization*

$$\mathbf{D}_{jj} = \boldsymbol{\Sigma}_{jj \mid \prec j}, \quad \mathbf{L}_{\prec j}] = -\boldsymbol{\Sigma}_{\prec j}^{-1} \boldsymbol{\Sigma}_{\prec j}], \quad \eta_j = \mu_j + \mathbf{L}_{\prec j}]^\top \boldsymbol{\mu}_{\prec j}, \quad j = 1, \dots, q.$$

Then $\perp\!\!\!\perp_j (\mathbf{D}_{jj}, \mathbf{L}_{\prec j}], \eta_j)$; in other words the triples $(\mathbf{D}_{jj}, \mathbf{L}_{\prec j}], \eta_j)$ are mutually stochastically independent.

Proof. Consider first the partition $\mathbf{x}^\top = (\mathbf{x}_{(1)}^\top \mathbf{x}_{(2)}^\top)$ with $\mathbf{x}_{(1)} = (x_q, \dots, x_2)^\top$ and $\mathbf{x}_{(2)} = x_1$ and for node $j = 1$ the re-parameterization

$$\begin{aligned} \mathbf{D}_{11} &= \boldsymbol{\Sigma}_{11 \mid \prec 1} \\ \mathbf{L}_{\prec 1}] &= -\boldsymbol{\Sigma}_{\prec 1}^{-1} \boldsymbol{\Sigma}_{\prec 1}] \\ \eta_1 &= \mu_1 + \mathbf{L}_{\prec 1}]^\top \boldsymbol{\mu}_{\prec 1}. \end{aligned}$$

Equivalently, we can write $\mathbf{D}_{11} = \boldsymbol{\Omega}_{(2)(2)}^{-1}$ and $\mathbf{L}_{\prec 1}] = \boldsymbol{\Omega}_{(2)(2)}^{-1} \boldsymbol{\Omega}_{(2)(1)}$.

Then, by applying Lemma 1.1 we obtain

$$(\boldsymbol{\mu}_{(1)}, \boldsymbol{\Omega}_{(1)(1) \mid (2)}) \perp\!\!\!\perp (\boldsymbol{\gamma}_{(2)}, \boldsymbol{\Omega}_{(1)(2)}, \boldsymbol{\Omega}_{(2)(2)}).$$

Moreover, because $\boldsymbol{\gamma}_{(2)} = \mu_1 + \mathbf{L}_{\prec 1}]^\top \boldsymbol{\mu}_{\prec 1} = \eta_1$, we can write

$$(\boldsymbol{\mu}_{(1)}, \boldsymbol{\Omega}_{(1)(1) \mid (2)}) \perp\!\!\!\perp (\mathbf{D}_{11}, \mathbf{L}_{\prec 1}], \eta_1).$$

Consider now the partition $\mathbf{x}^\top = (\mathbf{x}_{(1)}^\top \mathbf{x}_{(2)}^\top)$ with $\mathbf{x}_{(1)}^\top = (x_q, \dots, x_3)^\top$ and $\mathbf{x}_{(2)} = x_2$. Similarly as before, we can write $\mathbf{D}_{22} = \boldsymbol{\Omega}_{(2)(2)}^{-1}$, $\mathbf{L}_{\prec 2}] = \boldsymbol{\Omega}_{(2)(2)}^{-1} \boldsymbol{\Omega}_{(2)(1)}$ and $\eta_2 = \mu_2 + \mathbf{L}_{\prec 2}]^\top \boldsymbol{\mu}_{\prec 2}$. Therefore, from Lemma 1.1 we obtain

$$(\boldsymbol{\mu}_{(1)}, \boldsymbol{\Omega}_{(1)(1) \mid (2)}) \perp\!\!\!\perp (\mathbf{D}_{22}, \mathbf{L}_{\prec 2}], \eta_2),$$

so that

$$(\boldsymbol{\mu}_{(1)}, \boldsymbol{\Omega}_{(1)(1) \mid (2)}) \perp\!\!\!\perp (\mathbf{D}_{22}, \mathbf{L}_{\prec 2}], \eta_2) \perp\!\!\!\perp (\mathbf{D}_{11}, \mathbf{L}_{\prec 1}], \eta_1).$$

Proceeding iteratively until $\mathbf{x}_{(1)} = \emptyset$ and $\mathbf{x}_{(2)} = x_q$, so that $\mathbf{D}_{qq} = \boldsymbol{\Sigma}_{qq}$, $\mathbf{L}_{\prec q}] = \emptyset$, $\eta_q = \mu_q$, we obtain $\perp\!\!\!\perp_j (\mathbf{D}_{jj}, \mathbf{L}_{\prec j}], \eta_j)$ which proves global parameter independence. \square

Proposition 1.2 (Node-parameter distribution). *Let $(\boldsymbol{\mu}, \boldsymbol{\Omega}) \sim \mathcal{NW}_q(a_\mu, \mathbf{m}, a_\Omega, \mathbf{U})$, $a_\mu > 0, \mathbf{m} \in \mathbb{R}^q, a_\Omega > q - 1$ and \mathbf{U} s.p.d. Consider the re-parameterization*

$$\mathbf{D}_{jj} = \boldsymbol{\Sigma}_{jj| \prec j\succ}, \quad \mathbf{L}_{\prec j]} = -\boldsymbol{\Sigma}_{\prec j\succ}^{-1} \boldsymbol{\Sigma}_{\prec j]}, \quad \eta_j = \mu_j + \mathbf{L}_{\prec j]}^\top \boldsymbol{\mu}_{\prec j\succ}, \quad j = 1, \dots, q.$$

Then,

$$\begin{aligned} \mathbf{D}_{jj} &\sim \text{I-Ga} \left(\frac{1}{2} a_j^C, \frac{1}{2} \mathbf{U}_{jj| \prec j\succ} \right), \\ \mathbf{L}_{\prec j]} | \mathbf{D}_{jj} &\sim \mathcal{N}_{|\text{pa}(j)|} \left(-\mathbf{U}_{\prec j\succ}^{-1} \mathbf{U}_{\prec j]}, \mathbf{D}_{jj} \mathbf{U}_{\prec j\succ}^{-1} \right), \\ \eta_j | \mathbf{L}_{\prec j]}, \mathbf{D}_{jj} &\sim \mathcal{N} \left(m_j + \mathbf{L}_{\prec j]}^\top \mathbf{m}_{\prec j\succ}, \mathbf{D}_{jj}/a_\mu \right) \end{aligned}$$

where $a_j^C = a_\Omega + |\text{pa}(j)| - q + 1$.

Proof. Distributions of $\mathbf{L}_{\prec j]}$ and \mathbf{D}_{jj} follow from Theorem 7.1 in Ben-David et al. [1] where we also used the relationship

$$\begin{aligned} a_j &= a_\Omega + q - 2j + 3 \\ &= a_\Omega + q - 2(q - |\text{pa}(j)|) + 3 \\ &= a_\Omega - q + 2|\text{pa}(j)| + 3, \end{aligned}$$

which holds for complete DAGs with a parent ordering of the nodes so that $j = q - |\text{pa}(j)|$, and implies

$$\frac{a_j}{2} - \frac{|\text{pa}(j)|}{2} - 1 = \frac{a + |\text{pa}(j)| - q + 1}{2} := \frac{a_j^C}{2}.$$

Consider now $\eta_j = \mu_j + \mathbf{L}_{\prec j]}^\top \boldsymbol{\mu}_{\prec j\succ}$. Since $\boldsymbol{\mu} | \boldsymbol{\Omega} \sim \mathcal{N}_q(\mathbf{m}, (a_\mu \boldsymbol{\Omega})^{-1})$ and η_j is linear in μ_j and $\boldsymbol{\mu}_{\prec j\succ}$, the conditional distribution of η_j given $(\mathbf{L}_{\prec j]}, \mathbf{D}_{jj})$ is still Gaussian with mean

$$\mathbb{E}(\eta_j | \mathbf{L}_{\prec j]}, \mathbf{D}_{jj}) = m_j + \mathbf{L}_{\prec j]}^\top \mathbf{m}_{\prec j\succ}.$$

In addition,

$$\text{Var}(\eta_j | \mathbf{L}_{\prec j]}, \mathbf{D}_{jj}) = \text{Var}(\mu_j | \mathbf{D}_{jj}, \mathbf{L}_{\prec j}]) + \text{Var}(\mathbf{L}_{\prec j]}^\top \boldsymbol{\mu}_{\prec j\succ}) + 2\text{Cov}(\mu_j, \mathbf{L}_{\prec j]}^\top \boldsymbol{\mu}_{\prec j\succ}).$$

Using the fact that $\text{Cov}(\mathbf{A}^\top \mathbf{x}, \mathbf{B}^\top \mathbf{y}) = \mathbf{A}^\top \text{Cov}(\mathbf{x}, \mathbf{y}) \mathbf{B}$, for arbitrary $(p, 1)$ vectors \mathbf{x}, \mathbf{y} and (p, p) matrices \mathbf{A}, \mathbf{B} [6, Equation 8a.1.5] we can write

$$\text{Var}(\eta_j | \mathbf{L}_{\prec j]}, \mathbf{D}_{jj}) = \frac{1}{a_\mu} \left\{ \boldsymbol{\Sigma}_{jj} + \mathbf{L}_{\prec j]}^\top \boldsymbol{\Sigma}_{\prec j\succ} \mathbf{L}_{\prec j]} + 2\boldsymbol{\Sigma}_{[j\succ]} \mathbf{L}_{\prec j]} \right\} = \frac{1}{a_\mu} \mathbf{D}_{jj},$$

where we also used the relationships $\boldsymbol{\Sigma}_{jj| \prec j\succ} = \boldsymbol{\Sigma}_{jj} - \boldsymbol{\Sigma}_{[j\succ]} \boldsymbol{\Sigma}_{\prec j\succ}^{-1} \boldsymbol{\Sigma}_{\prec j]}$ and $\mathbf{L}_{\prec j]} = -\boldsymbol{\Sigma}_{\prec j\succ}^{-1} \boldsymbol{\Sigma}_{\prec j}$. Hence,

$$\eta_j | \mathbf{L}_{\prec j]}, \mathbf{D}_{jj} \sim \mathcal{N} \left(m_j + \mathbf{L}_{\prec j]}^\top \mathbf{m}_{\prec j\succ}, \mathbf{D}_{jj}/a_\mu \right).$$

□

1.2 Arbitrary DAGs

Let now \mathcal{D} be an arbitrary (typically not complete) DAG and assume a parent ordering of its nodes. For each $j \in \{1, \dots, q\}$, let $\boldsymbol{\theta}_j = \{\mathbf{D}_{jj}, \mathbf{L}_{\prec j}], \eta_j\}$ be the parameters associated to node j , and identify a *complete* DAG $\mathcal{D}^{C(j)}$ such that $\text{pa}_{\mathcal{D}^{C(j)}}(j') = \text{pa}_{\mathcal{D}}(j)$, where j' in $\mathcal{D}^{C(j)}$ corresponds to the same variable as j in \mathcal{D} . Because of the parent ordering $j' = q - |\text{pa}_{\mathcal{D}}(j)|$ which is usually different from j . Let $\boldsymbol{\theta}_{j'}^{C(j)}$ be the parameter of node j' under the complete DAG $\mathcal{D}^{C(j)}$. Following the procedure of G&H we then assign to $\boldsymbol{\theta}_j$ the same prior of $\boldsymbol{\theta}_{j'}^{C(j)}$ which can be gathered from Equation (3) in the complete Normal-DAG-Wishart version. In particular, for a given DAG \mathcal{D} we obtain

$$\begin{aligned} \mathbf{D}_{jj} &\sim \text{I-Ga}\left(\frac{1}{2}a_j^{\mathcal{D}}, \frac{1}{2}\mathbf{U}_{jj|\prec j}\right), \\ \mathbf{L}_{\prec j}] | \mathbf{D}_{jj} &\sim \mathcal{N}_{|\text{pa}_{\mathcal{D}}(j)|}\left(-\mathbf{U}_{\prec j}^{-1}\mathbf{U}_{\prec j}], \mathbf{D}_{jj}\mathbf{U}_{\prec j}^{-1}\right), \\ \eta_j | \mathbf{L}_{\prec j}], \mathbf{D}_{jj} &\sim \mathcal{N}\left(m_j + \mathbf{L}_{\prec j}^{\top}\mathbf{m}_{\prec j}, \mathbf{D}_{jj}/a_{\mu}\right), \end{aligned} \quad (3)$$

where $a_j^{\mathcal{D}} = a_{\Omega} + |\text{pa}_{\mathcal{D}}(j)| - q + 1$. Notice that all distributions in (3) only depend on the cardinality of $\text{pa}_{\mathcal{D}}(j)$ which is the same across alternative parent orderings. Finally, by assuming independence among node-parameters $(\mathbf{D}_{jj}, \mathbf{L}_{\prec j}], \eta_j)$, we can write

$$p(\mathbf{D}, \mathbf{L}, \boldsymbol{\eta}) = \prod_{j=1}^q p(\mathbf{D}_{jj}, \mathbf{L}_{\prec j}], \eta_j). \quad (4)$$

1.3 Posterior distribution

We now derive the posterior distribution of DAG node-parameters $(\mathbf{D}_{jj}, \mathbf{L}_{\prec j}], \eta_j)$, $j = 1, \dots, q$. For expediency, we proceed by computing first the posterior on the parameters $(\boldsymbol{\mu}, \boldsymbol{\Omega})$ under a complete DAG model $\mathcal{N}_q(\boldsymbol{\mu}, \boldsymbol{\Omega}^{-1})$, $\boldsymbol{\Omega} \in \mathcal{P}$, which by conjugacy is still Normal-Wishart, and then recover, through the procedure of G&H, the posterior on node-parameters. In particular, given n i.i.d. q -dimensional samples $\mathbf{x}_1, \dots, \mathbf{x}_n$ collected in the (n, q) data matrix \mathbf{X} , we have

$$\boldsymbol{\mu} | \boldsymbol{\Omega}, \mathbf{X} \sim \mathcal{N}_q(\tilde{\mathbf{m}}, (\tilde{a}_{\mu}\boldsymbol{\Omega})^{-1}), \quad \boldsymbol{\Omega} | \mathbf{X} \sim \mathcal{W}_q(\tilde{a}_{\Omega}, \tilde{\mathbf{U}}).$$

with $\tilde{a}_{\mu} = a_{\mu} + n$, $\tilde{a}_{\Omega} = a_{\Omega} + n$, and

$$\begin{aligned} \tilde{\mathbf{m}} &= \frac{a_{\mu}}{a_{\mu} + n}\mathbf{m} + \frac{n}{a_{\mu} + n}\bar{\mathbf{x}}, \\ \tilde{\mathbf{U}} &= \mathbf{U} + \mathbf{S} + \frac{a_{\mu}n}{a_{\mu} + n}\mathbf{S}_0, \end{aligned}$$

where $\mathbf{S} = \sum_{i=1}^n (\mathbf{x}_i - \bar{\mathbf{x}})(\mathbf{x}_i - \bar{\mathbf{x}})^{\top}$, $\mathbf{S}_0 = (\bar{\mathbf{x}} - \mathbf{m})(\bar{\mathbf{x}} - \mathbf{m})^{\top}$ and $\bar{\mathbf{x}}$ is the $(q, 1)$ vector collecting the sample means of X_1, \dots, X_q . Therefore, the posterior distribution of the DAG node-parameters $(\mathbf{D}_{jj}, \mathbf{L}_{\prec j}], \eta_j)$ can be retrieved from (3) simply by updating the hyperparameters as $a_{\mu} \mapsto \tilde{a}_{\mu}$, $a_{\Omega} \mapsto \tilde{a}_{\Omega}$, $\mathbf{m} \mapsto \tilde{\mathbf{m}}$, $\mathbf{U} \mapsto \tilde{\mathbf{U}}$.

1.4 Marginal data distribution

Consider the Gaussian DAG model $X_1, \dots, X_q | \boldsymbol{\mu}, \boldsymbol{\Omega} \sim \mathcal{N}_q(\boldsymbol{\mu}, \boldsymbol{\Omega}^{-1})$, $\boldsymbol{\Omega} \in \mathcal{P}_{\mathcal{D}}$ and the re-parameterization $(\boldsymbol{\mu}, \boldsymbol{\Omega}) \mapsto (\mathbf{D}, \mathbf{L}, \boldsymbol{\eta})$. The likelihood function can be written as

$$f(\mathbf{X} | \mathbf{D}, \mathbf{L}, \boldsymbol{\eta}, \mathcal{D}) = \prod_{j=1}^q d\mathcal{N}_n(\mathbf{X}_j | \eta_j \mathbf{1}_n - \mathbf{X}_{\text{pa}_{\mathcal{D}}(j)} \mathbf{L}_{\prec j}], D_{jj} \mathbf{I}_n), \quad (5)$$

where $\mathbf{1}_n$ is the $(n, 1)$ unit vector and \mathbf{I}_n the (n, n) identity matrix. Because of parameter prior independence in (4) the marginal likelihood of DAG \mathcal{D} admits the same node-by-node factorization, namely

$$m(\mathbf{X} | \mathcal{D}) = \int f(\mathbf{X} | \mathbf{D}, \mathbf{L}, \boldsymbol{\eta}, \mathcal{D}) p(\mathbf{D}, \mathbf{L}, \boldsymbol{\eta}) d(\mathbf{D}, \mathbf{L}, \boldsymbol{\eta}) \quad (6)$$

$$= \prod_{j=1}^q m(\mathbf{X}_j | \mathbf{X}_{\text{pa}_{\mathcal{D}}(j)}, \mathcal{D}). \quad (7)$$

In addition, because of conjugacy of the prior $p(\mathbf{D}_{jj}, \mathbf{L}_{\prec j}], \eta_j)$ with the Normal density $d\mathcal{N}_n(\mathbf{X}_j | \cdot)$, each term $m(\mathbf{X}_j | \mathbf{X}_{\text{pa}_{\mathcal{D}}(j)}, \mathcal{D})$ can be obtained in closed-form expression from the ratio of prior and posterior normalizing constants as

$$m(\mathbf{X}_j | \mathbf{X}_{\text{pa}_{\mathcal{D}}(j)}, \mathcal{D}) = (2\pi)^{-\frac{n}{2}} \cdot \frac{a_{\mu}^{\frac{1}{2}}}{\tilde{a}_{\mu}^{\frac{1}{2}}} \cdot \frac{|\mathbf{U}_{\prec j}^{\mathcal{D}}|^{\frac{1}{2}}}{|\tilde{\mathbf{U}}_{\prec j}^{\mathcal{D}}|^{\frac{1}{2}}} \cdot \frac{\Gamma\left(\frac{1}{2}\tilde{a}_j^{\mathcal{D}}\right)}{\Gamma\left(\frac{1}{2}a_j^{\mathcal{D}}\right)} \cdot \frac{\left(\frac{1}{2}\mathbf{U}_{jj} | \prec j\right)^{\frac{1}{2}a_j^{\mathcal{D}}}}{\left(\frac{1}{2}\tilde{\mathbf{U}}_{jj} | \prec j\right)^{\frac{1}{2}\tilde{a}_j^{\mathcal{D}}}}, \quad (8)$$

where $\tilde{a}_j^{\mathcal{D}} = \tilde{a}_{\Omega} + |\text{pa}_{\mathcal{D}}(j)| - q + 1$.

2 MCMC sampler

In this section we provide full details on the MCMC scheme that we adopt for posterior inference on our model. For completeness, we also summarize some basic concepts on DP mixture models.

Definition 2.1. *A random distribution H follows a Dirichlet process (DP) with parameters α_0 (precision) and M (baseline), written $H(\cdot) \sim DP(\alpha_0, M)$, if*

- $H(\cdot) = \sum_{k=1}^{\infty} \omega_k \delta_{(\boldsymbol{\theta}_k^*)}(\cdot)$, with $\theta_1^*, \theta_2^*, \dots \stackrel{\text{iid}}{\sim} M$,
- $\omega_k = v_k \prod_{s < k} (1 - v_s)$, with $v_1, v_2, \dots \stackrel{\text{iid}}{\sim} \text{Beta}(1, \alpha_0)$.

In our setting $\boldsymbol{\theta}_k^*$ is represented by the triple $(\boldsymbol{\mu}_k^*, \boldsymbol{\Omega}_k^*, \mathcal{D}_k^*)$, namely the mean vector and precision matrix $(\boldsymbol{\mu}_k^*, \boldsymbol{\Omega}_k^*)$ corresponding to the DAG \mathcal{D}_k^* . Moreover, $\{\omega_k\}_{k=1}^{\infty}$ are weights satisfying $\omega_k \in (0, 1)$ and $\sum_{k=1}^{\infty} \omega_k = 1$. Therefore, sampling from H is equivalent to drawing from the set $\{\boldsymbol{\theta}_k^*\}$'s with probability ω_k , $k = 1, \dots, \infty$.

Let now X_1, \dots, X_q be a collection of real-valued random variables. Conditionally on the discrete random measure H , we assume that the vector (X_1, \dots, X_q) follows a DP mixture of Gaussian DAG models, namely

$$\begin{aligned} X_1, \dots, X_q | H &\sim \int f(x_1, \dots, x_q | \boldsymbol{\mu}, \boldsymbol{\Omega}, \mathcal{D}) H(d\boldsymbol{\mu}, d\boldsymbol{\Omega}, d\mathcal{D}) \\ H &\sim \text{DP}(\alpha_0, M), \end{aligned} \tag{9}$$

where $f(x_1, \dots, x_q | \boldsymbol{\mu}, \boldsymbol{\Omega}, \mathcal{D})$ denotes the density of a Gaussian DAG model, as defined in Section 2.2 of our paper. With regard to the baseline measure we set

$$M(d\boldsymbol{\mu}, d\boldsymbol{\Omega}, d\mathcal{D}) = p(\boldsymbol{\mu}, \boldsymbol{\Omega} | \mathcal{D}) p(\mathcal{D}) d\boldsymbol{\mu} d\boldsymbol{\Omega} d\mathcal{D} \tag{10}$$

with priors $p(\boldsymbol{\mu}, \boldsymbol{\Omega} | \mathcal{D})$ and $p(\mathcal{D})$ defined in Section 3.1 of our paper. Let now $\mathbf{x}_i = (x_{i,1}, \dots, x_{i,q})^\top$, $i = 1, \dots, n$, be n independent draws from (9). Recall that in a DP mixture each sample \mathbf{x}_i , $i = 1, \dots, n$, has potentially a distinct parameter $\boldsymbol{\theta}_i = (\boldsymbol{\mu}_i, \boldsymbol{\Omega}_i, \mathcal{D}_i)$. Let $K \leq n$ be the unique values among $\boldsymbol{\theta}_1, \dots, \boldsymbol{\theta}_n$ and ξ_1, \dots, ξ_n a sequence of indicator variables, with $\xi_i \in \{1, \dots, K\}$, such that $\boldsymbol{\theta}_i = \boldsymbol{\theta}_{\xi_i}^*$. Denote now with \mathbf{X} the (n, q) data matrix obtained by row-binding the individual observations \mathbf{x}_i^\top 's. The DP mixture model can be written in terms of the random partition induced by the $\{\xi_i\}$'s

$$f(\mathbf{X} | \xi_1, \dots, \xi_n, K) = \prod_{k=1}^K \left\{ \int \left[\prod_{i: \xi_i=k} f(\mathbf{x}_i | \boldsymbol{\mu}_k^*, \boldsymbol{\Omega}_k^*, \mathcal{D}_k^*) \right] M(d\boldsymbol{\mu}_k^*, d\boldsymbol{\Omega}_k^*, d\mathcal{D}_k^*) \right\}. \tag{11}$$

To sample from the posterior of the DP mixture we rely on the *slice sampler* [7]; see also Kalli et al. [5]. Recall that the likelihood function in Equation (11) and the prior on parameters defined in Sections 3.1 and 3.2, where in particular $\boldsymbol{\theta}_k^* \stackrel{iid}{\sim} M$. We introduce auxiliary variables $\{v_k\}_{k=1}^\infty$ such that $v_k \stackrel{iid}{\sim} \text{Beta}(1, \alpha_0)$ and $\omega_k = v_k \prod_{h < k} (1 - v_h)$, where ω_k 's are the weights of the DP; see also Section 3. Let also u_1, \dots, u_n be uniformly distributed auxiliary variables such that

$$\begin{aligned} p(u_i, \mathbf{x}_i, \xi_i | \mathbf{v}, \boldsymbol{\theta}_i^*) &= f(\mathbf{x}_i | \boldsymbol{\theta}_{\xi_i}^*) \mathbb{1}(u_i < \omega_{\xi_i}) \\ &= f(\xi_i | \mathbf{v}) f(u_i | \xi_i, \mathbf{v}) f(\mathbf{x}_i | \boldsymbol{\theta}_{\xi_i}^*). \end{aligned}$$

The *augmented* joint distribution of the data and parameters can be written as

$$f(\mathbf{X}, \mathbf{u}, \mathbf{v}, \boldsymbol{\xi}, \boldsymbol{\theta}^*, \alpha_0) = \prod_{i=1}^n \{f(\xi_i | \mathbf{v}) f(u_i | \xi_i, \mathbf{v}) f(\mathbf{x}_i | \boldsymbol{\theta}_{\xi_i}^*)\} \prod_{k=1}^K p(v_k) \prod_{k=1}^K p(\boldsymbol{\theta}_k^*) \cdot p(\alpha_0)$$

where $\mathbf{u} = (u_1, \dots, u_n)^\top$ and $\boldsymbol{\xi} = (\xi_1, \dots, \xi_n)^\top$. Update of parameters $(\mathbf{u}, \mathbf{v}, \boldsymbol{\xi}, \boldsymbol{\theta}^*)$ is performed in the following steps.

2.1 Update of (\mathbf{u}, \mathbf{v})

Block-update of parameters (\mathbf{u}, \mathbf{v}) is performed by sampling from their joint full conditional distribution $f(\mathbf{u}, \mathbf{v} | \cdot) = f(\mathbf{u} | \mathbf{v}, \cdot) f(\mathbf{v} | \cdot)$. In particular, we have

$$f(\mathbf{u} | \mathbf{v}, \cdot) \propto \prod_{i=1}^n f(u_i | \xi_i, \mathbf{v}) = \prod_{i=1}^n \mathbb{1}(u_i < \omega_{\xi_i}),$$

so that u_i 's are mutually independent a posteriori with distribution

$$u_i | \cdot \sim \text{Unif}(0, \omega_{\xi_i}), \quad i = 1, \dots, n.$$

Moreover,

$$f(\mathbf{v} | \cdot) \propto \prod_{i=1}^n \{f(\xi_i | \mathbf{v}) f(u_i | \xi_i, \mathbf{v})\} p(v_k).$$

Recalling that $\omega_k = v_k \prod_{h < k} (1 - v_h)$, $v_k \sim \text{Beta}(1, \alpha_0)$ and $\Pr(\xi_i = k | \mathbf{v}) = \omega_k$ we can write

$$\begin{aligned} f(v_k | \cdot) &\propto \prod_{i=1}^n \left\{ v_{\xi_i} \prod_{h < \xi_i} (1 - v_h) \right\} (1 - v_k)^{\alpha_0 - 1} \\ &= \prod_{k=1}^K \prod_{i: \xi_i=k} \left\{ v_k \prod_{v < h} (1 - v_h) \right\} (1 - v_k)^{\alpha_0 - 1}, \end{aligned}$$

where $K = \max\{\xi_i, i = 1, \dots, n\}$. It is then straightforward to show that v_1, \dots, v_K are mutually independent with distribution

$$v_k | \dots \sim \text{Beta} \left(n_k + 1, \alpha_0 + \sum_{h > k} n_h \right), \quad k = 1, \dots, K,$$

while $v_k \sim \text{Beta}(1, \alpha_0)$ for any $k > K$.

2.2 Update of indicator variables ξ_1, \dots, ξ_n

The full conditional distribution of indicator variables ξ_i is such that

$$\Pr\{\xi_i = k | \cdot\} \propto f(\mathbf{x}_i | \boldsymbol{\theta}_{\xi_i}^*) \mathbb{1}(u_i < \omega_{\xi_i}) \propto \begin{cases} f(\mathbf{x}_i | \boldsymbol{\theta}_i^*) & u_i < \omega_{\xi_i}, \\ 0 & \text{otherwise.} \end{cases}$$

2.3 Update of DAG and Cholesky parameters

Under the full conditional distribution the cluster-specific parameters $\{\boldsymbol{\theta}_k^* = (\boldsymbol{\mu}_k^*, \boldsymbol{\Omega}_k^*, \mathcal{D}_k^*), k = 1, 2, \dots\}$ are mutually stochastically independent. We can therefore update separately each component, and obtain

$$p(\boldsymbol{\theta}_k^* | \cdot) \propto \begin{cases} \prod_{i: \xi_i=k} f(\mathbf{x}_i | \boldsymbol{\theta}_k^*) p(\boldsymbol{\theta}_k^*) & \text{if } k \leq \max\{\xi_i, i = 1, \dots, n\}, \\ p(\boldsymbol{\theta}_k^*) & \text{otherwise.} \end{cases} \quad (12)$$

Notice that in the second line of (12) we require to sample from the baseline over DAGs and parameters; see Section 2.5 for details. Write now $\prod_{i:\xi_i=k} f(\mathbf{x}_i | \boldsymbol{\theta}_k^*) = f(\mathbf{X}^{(k)} | \boldsymbol{\theta}_k^*)$, where $\mathbf{X}^{(k)}$ is the (n_k, q) matrix collecting only those observations \mathbf{x}_i 's such that $\xi_i = k$. Without loss of generality, consider a generic cluster and omit for simplicity subscripts k and “*” from $\boldsymbol{\theta}_k^*$ and $\mathbf{X}^{(k)}$. Update of $\boldsymbol{\theta} = (\boldsymbol{\mu}, \boldsymbol{\Omega}, \mathcal{D})$ can be performed by resorting to an MCMC scheme based on a *Partial Analytic Structure* (PAS) algorithm [4]. Consider first the re-parameterization $(\boldsymbol{\mu}, \boldsymbol{\Omega}) \mapsto (\mathbf{D}, \mathbf{L}, \boldsymbol{\eta})$. The update of DAG \mathcal{D} and parameters $(\mathbf{D}, \mathbf{L}, \boldsymbol{\eta})$ is then performed in two steps.

In the first step, for a given DAG \mathcal{D} , a new DAG $\tilde{\mathcal{D}}$ is proposed from a suitable proposal distribution which is defined as follows. We consider three types of operators that locally modify a DAG: insert a directed edge (InsertD $u \rightarrow v$ for short), delete a directed edge (DeleteD $u \rightarrow v$) and reverse a directed edge (ReverseD $u \rightarrow v$). For a given $\mathcal{D} \in \mathcal{S}_q$, where \mathcal{S}_q is the set of all DAGs on q nodes, we construct the set of valid operators $\mathcal{O}_{\mathcal{D}}$, that is operators whose resulting graph is a DAG. A DAG $\tilde{\mathcal{D}}$ is then called a *direct successor* of \mathcal{D} if it can be reached by applying an operator in $\mathcal{O}_{\mathcal{D}}$ to \mathcal{D} . Therefore, given the current \mathcal{D} we propose $\tilde{\mathcal{D}}$ by uniformly sampling an element in $\mathcal{O}_{\mathcal{D}}$ and applying it to \mathcal{D} . Since there is a one-to-one correspondence between each operator and the resulting DAG, the probability of transition is $q(\tilde{\mathcal{D}} | \mathcal{D}) = 1/|\mathcal{O}_{\mathcal{D}}|$, for each $\tilde{\mathcal{D}}$ direct successor of \mathcal{D} . For any two DAGs \mathcal{D} and $\tilde{\mathcal{D}}$ differing by one edge $(u, v) \in \mathcal{D}$, $(u, v) \notin \tilde{\mathcal{D}}$, it can be shown that the acceptance probability for $\tilde{\mathcal{D}}$ under a PAS algorithm is given by $\alpha_{\tilde{\mathcal{D}}} = \min\{1; r_{\tilde{\mathcal{D}}}\}$ with

$$r_{\tilde{\mathcal{D}}} = \frac{m(\mathbf{X}_v | \mathbf{X}_{\text{pa}_{\tilde{\mathcal{D}}}(v)}, \tilde{\mathcal{D}})}{m(\mathbf{X}_v | \mathbf{X}_{\text{pa}_{\mathcal{D}}(v)}, \mathcal{D})} \cdot \frac{p(\tilde{\mathcal{D}})}{p(\mathcal{D})} \cdot \frac{q(\mathcal{D} | \tilde{\mathcal{D}})}{q(\tilde{\mathcal{D}} | \mathcal{D})}, \quad (13)$$

with $m(\mathbf{X}_v | \mathbf{X}_{\text{pa}_{\tilde{\mathcal{D}}}(v)}, \tilde{\mathcal{D}})$ as in Equation (8).

In the second step we then sample $(\mathbf{D}, \mathbf{L}, \boldsymbol{\eta})$ conditionally on the accepted DAG, say \mathcal{D} , from its full conditional distribution. The latter reduces to

$$p(\mathbf{D}, \mathbf{L}, \boldsymbol{\eta} | \mathbf{X}, \mathcal{D}) = \prod_{j=1}^q p(\mathbf{D}_{jj}, \mathbf{L}_{\prec j}, \eta_j | \mathbf{X}, \mathcal{D}),$$

where dependence on \mathcal{D} has been made explicit. Its expression can be recovered from the posterior of node-parameters in Section 1.3.

2.4 Update of precision parameter α_0

A useful property of the DP mixture model is that α_0 is conditionally independent of \mathbf{X} given K , parameters $\{\boldsymbol{\theta}_i\}_{i=1}^n$, and indicator variables $\{\xi_i\}_{i=1}^n$ [2]. Furthermore, $\{\boldsymbol{\theta}_i\}_{i=1}^n$ are also conditionally independent of α_0 given K and the indicator variables. Therefore, the full conditional

distribution of α_0 reduces to $p(\alpha_0 | K) \propto p(\alpha_0)p(K | \alpha_0)$, where

$$p(K | \alpha_0) = c_n(K)n! \alpha_0^K \frac{\Gamma(\alpha_0)}{\Gamma(\alpha_0 + n)}$$

is the prior on K implied by the DP and $c_n(K)$ is a normalizing constant not involving α_0 ; see again Escobar & West [2]. In particular, it can be shown that the conditional posterior of α_0 is a mixture of two Gamma densities

$$\alpha_0 | \eta, K \propto g \cdot \text{Gamma}(c + K, d - \log \eta) + (1 - g) \cdot \text{Gamma}(c + K - 1, d - \log \eta), \quad (14)$$

where $g/(1 - g) = (c + K - 1)/[n(d - \log \eta)]$ and $\eta \sim \text{Beta}(\alpha_0 + 1, n)$. As a consequence, at each step of the MCMC, update of α_0 is performed by i) sampling η conditionally on the current value of α_0 from $\text{Beta}(\alpha_0 + 1, n)$; ii) sampling a new value for α_0 conditionally on η and K from (14).

2.5 Sampling from the baseline over DAGs

Since the enumeration of all DAGs on q nodes is unfeasible in practice, direct sampling from the baseline $p(\mathcal{D})$ can be achieved by adopting the following MCMC strategy. For a given DAG \mathcal{D} let $N(\mathcal{D})$ be the set of all its direct successors, each one obtained by applying an operator in the set $\mathcal{O}_{\mathcal{D}}$ defined in Section 2.3. We first uniformly sample a DAG $\tilde{\mathcal{D}}$ from $N(\mathcal{D})$ that is with probability $q(\tilde{\mathcal{D}} | \mathcal{D}) = 1/|N(\mathcal{D})|$, for each $\tilde{\mathcal{D}} \in N(\mathcal{D})$. Hence, we move to $\tilde{\mathcal{D}}$ with probability

$$\alpha_{\tilde{\mathcal{D}}} = \min \left\{ 1, \frac{p(\tilde{\mathcal{D}})}{p(\mathcal{D})} \cdot \frac{q(\mathcal{D} | \tilde{\mathcal{D}})}{q(\tilde{\mathcal{D}} | \mathcal{D})} \right\}.$$

Notice the similarity with the acceptance ratio in (13); clearly, the difference is that here we are sampling from the *prior* over \mathcal{S}_q (the set of all DAGs on q nodes) and therefore no data are involved. Also, to compute $\alpha_{\tilde{\mathcal{D}}}$ we only need to evaluate the *ratio* of the priors $p(\tilde{\mathcal{D}})/p(\mathcal{D}) = r$, which does not require the computation of normalizing constants over the space of DAGs and is directly available from Equation (16) in our paper. Moreover, the ratio of the two proposal reduces to $q(\mathcal{D} | \tilde{\mathcal{D}})/q(\tilde{\mathcal{D}} | \mathcal{D}) = |\mathcal{O}_{\mathcal{D}}|/|\mathcal{O}_{\tilde{\mathcal{D}}}|$ which instead requires the enumeration of all the direct successors of \mathcal{D} and $\tilde{\mathcal{D}}$. While this is feasible with a relatively small computational cost, it was observed empirically that the approximation $q(\mathcal{D} | \tilde{\mathcal{D}})/q(\tilde{\mathcal{D}} | \mathcal{D}) \approx 1$ does not produce a relevant loss in terms of accuracy.

3 Analysis of gene expressions from GBM patients: diagnostics of convergence and additional results

3.1 Convergence diagnostics

To assess the convergence of our MCMC algorithm on the GBM data we ran two independent chains. Under both replicates we set prior hyperparameters as in Section 6 of our paper and fix

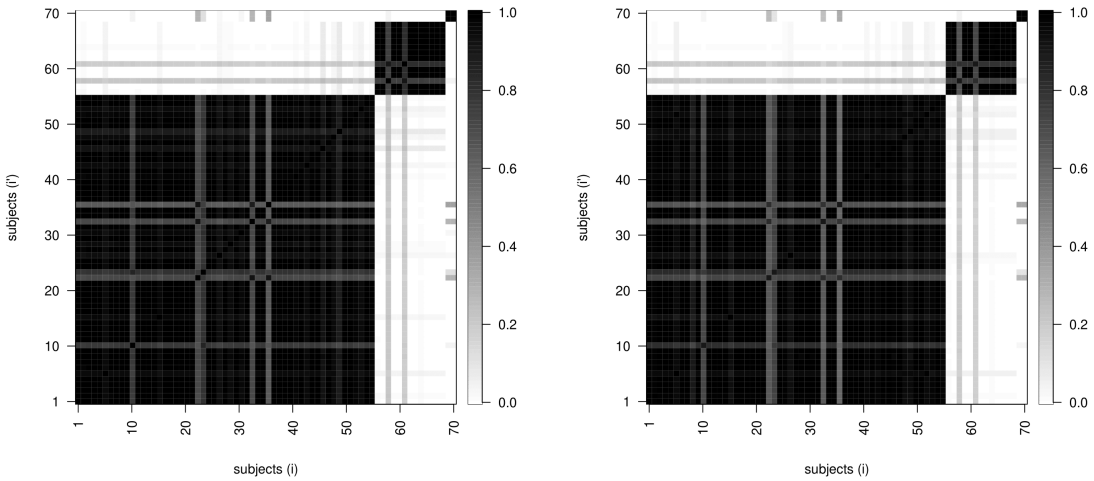


Figure 1: GBM data. Posterior similarity matrices obtained from two independent MCMC chains. Subjects arranged by cluster membership.

the number of MCMC iterations to $S = 120000$, which includes a burn-in period of 20000 runs.

For each of the two MCMC outputs we first produce an (n, n) similarity matrix based on the approximate posterior probabilities in Equation (17) of our paper, computed for each pair of subjects $(i, i'), i \neq i'$. The two resulting matrices are represented as heat-maps in Figure 1. By inspection, it appears that the agreement between the two outputs is highly satisfactory. Importantly, the two cluster structures, obtained by fixing a threshold for inclusion of 0.5, coincide.

Under each MCMC output, we then produce the collection of subject-specific BMA causal effect estimates. Figure 2 shows the scatter plots of causal effect estimates for response nodes $\text{TGF}\beta\text{R1}$ and $\text{TGF}\beta\text{3}$ (computed across all possible intervened nodes) obtained from the two MCMC chains. One can see that the agreement between the two outputs is highly satisfactory, since points lie close to the 45-degree reference line.

3.2 Comparison with *One-group naive* strategy

To appreciate the role played by population heterogeneity in causal effect estimation, we compare our results with a naive strategy which assumes that all observations are conditionally iid from the same one-component model. We call the resulting method *One-group naive*; see also Section 5.3 in our paper. Differently from our method, *One-group naive* does not rely on a DP mixture model, because it assumes that all observations belong to the same (unique) cluster. Apart from this, it is implemented using the same prior specifications on DAG- and parameter space adopted in our paper.

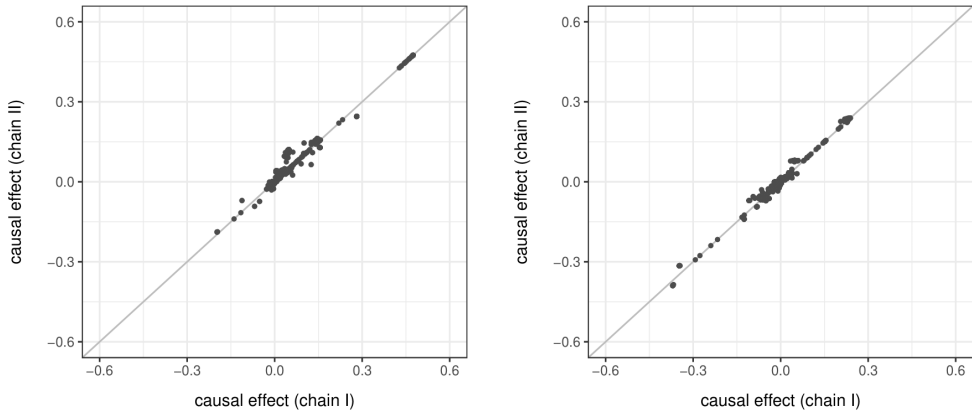


Figure 2: GBM data. Scatter plots of the BMA estimates for response nodes $\text{TGF}\beta\text{R1}$ (left) and $\text{TGF}\beta 3$ (right) obtained from two independent MCMC chains.

Results on causal effect estimation are summarized in Figures 3 and 4. Each heat-map reports the collection of subject-specific BMA estimates of causal effects on one response gene among $\text{TGF}\beta 1$, $\text{TGF}\beta 2$, $\text{TGF}\beta 3$, $\text{TGF}\beta\text{R1}$, $\text{TGF}\beta\text{R2}$ following an intervention on any other of the 20 genes involved in the pathway. Left-side plots were obtained from our DP mixture model. Right-side plots instead report the same collection of causal effects obtained from *One-group naive* strategy. Clearly, in the latter setting causal effects relative to each intervened node are equal across subjects. This output reveals substantial differences between the two strategies, suggesting that methods which neglect population heterogeneity can produce badly “biased” estimates. In particular, the one-group assumption has in some cases a “dilution” effect on coefficients’ estimates. This means that each causal effect obtained from *One-group naive* is akin to an average of cluster-specific causal estimates which are substantially different among groups. This happens for instance with regard to response $\text{TGF}\beta 1$ for causal effects associated with proteins of the SMAD family. Here, the causal effect obtained from *One-group naive* corresponds to a value in between the collection of causal effects resulting from DP mixture. As a consequence the ensuing causal effect coefficient provides an inadequate quantification of the underlying effect because it under- and over- estimates causal effects for individuals in clusters 1 and 2 respectively. In other cases, however, this does not happen and the differences between the *One-group naive* causal effect estimates and those in the mixture setting become hard to disentangle; see for instance the causal effects associated with proteins of the SMAD family for response $\text{TGF}\beta 2$, or the causal effect associated to SMAD4 when the response is $\text{TGF}\beta\text{R2}$.

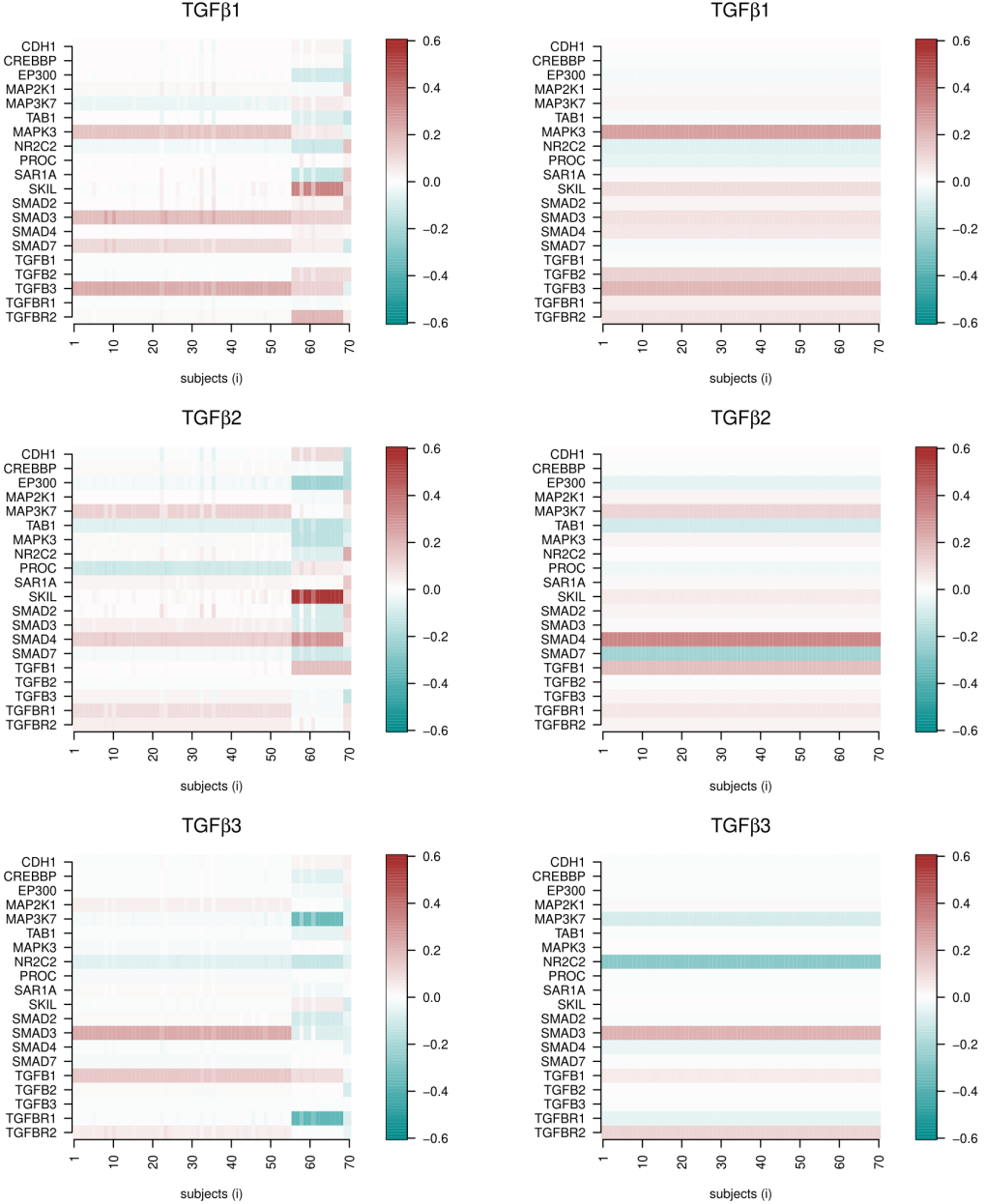


Figure 3: GBM data. Heat maps of causal effects on responses TGF β 1, TGF β 2, TGF β 3, following an intervention on one target gene among the twenty involved in the TGF β pathway. Subjects arranged by cluster membership under *DP mixture*. Left column: results obtained from our DP mixture model. Right column: results from *One-group naive* strategy.

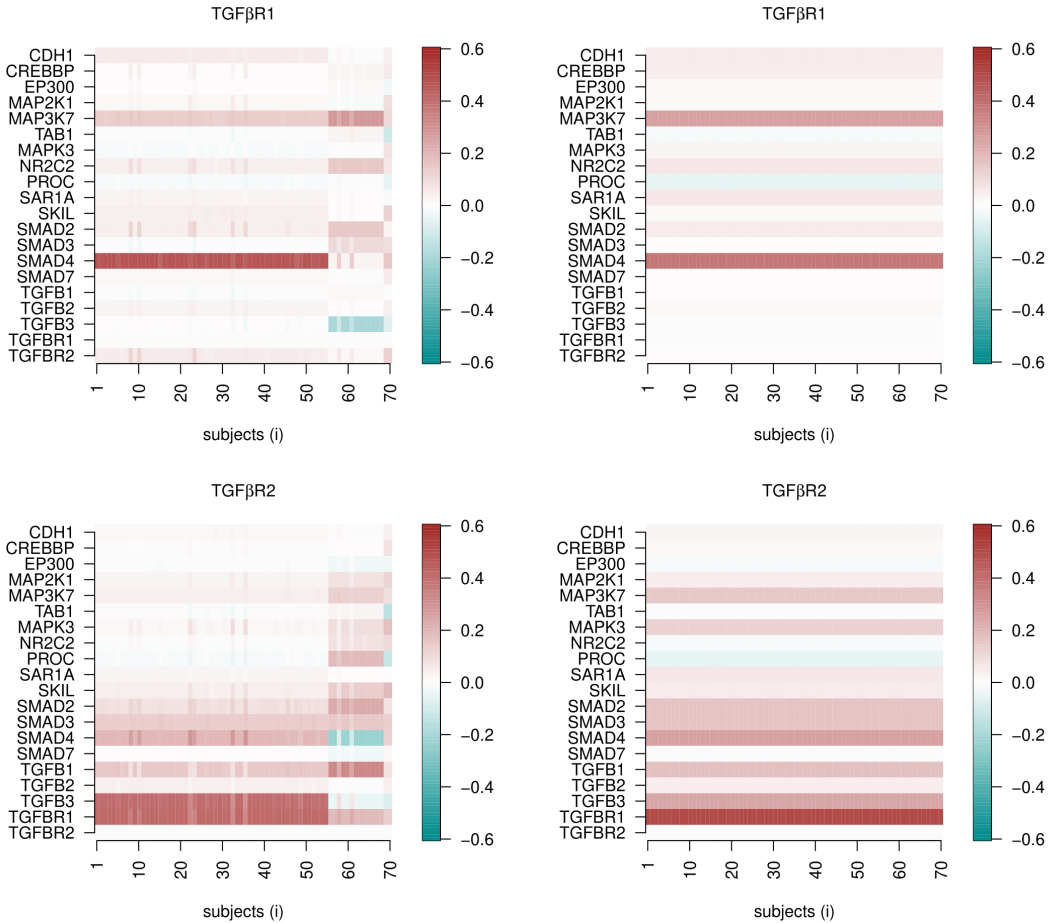


Figure 4: GBM data. Heat maps of causal effects on responses $TGF\beta R1$, $TGF\beta R2$, following an intervention on one target gene among the twenty involved in the $TGF\beta$ pathway. Subjects arranged by cluster membership under *DP mixture*. Left column: results obtained from our DP mixture model. Right column: results from *One-group naive* strategy.

References

- [1] BEN-DAVID, E., LI, T., MASSAM, H. & RAJARATNAM, B. (2015). High Dimensional Bayesian Inference for Gaussian Directed Acyclic Graph Models. *arXiv pre-print* URL <https://arxiv.org/abs/1109.4371>.
- [2] ESCOBAR, M. D. & WEST, M. (1995). Bayesian Density Estimation and Inference Using Mixtures. *Journal of the American Statistical Association* 90 577–588.
- [3] GEIGER, D. & HECKERMAN, D. (2002). Parameter Priors for Directed Acyclic Graphical Models and the Characterization of Several Probability Distributions. *The Annals of Statistics* 30 1412–1440.
- [4] GODSILL, S. J. (2012). On the Relationship Between Markov Chain Monte Carlo Methods for Model Uncertainty. *Journal of Computational and Graphical Statistics* 10 230–248.
- [5] KALLI, M., GRIFFIN, J. E. & WALKER, S. G. (2011). Slice Sampling Mixture Models. *Statistics and Computing* 21 93–105.
- [6] RAO, C. R. (1973). *Linear Statistical Inference and its Applications: 2nd edition*. John Wiley & Sons, Inc.
- [7] WALKER, S. G. (2007). Sampling the Dirichlet Mixture Model with Slices. *Communications in Statistics - Simulation and Computation* 36 45–54.